

Filtration of Hanford Tank 241-AW-105 Supernatant at 16 °C

May 2025

JR Allred
C Alvarez
AA Bachman
EC Buck
CA Burns
RC Daniel
JE Turner
RA Peterson

DISCLAIMER

This report was prepared as an account of work sponsored by an agency of the United States Government. Neither the United States Government nor any agency thereof, nor Battelle Memorial Institute, nor any of their employees, makes **any warranty, express or implied, or assumes any legal liability or responsibility for the accuracy, completeness, or usefulness of any information, apparatus, product, or process disclosed, or represents that its use would not infringe privately owned rights.** Reference herein to any specific commercial product, process, or service by trade name, trademark, manufacturer, or otherwise does not necessarily constitute or imply its endorsement, recommendation, or favoring by the United States Government or any agency thereof, or Battelle Memorial Institute. The views and opinions of authors expressed herein do not necessarily state or reflect those of the United States Government or any agency thereof.

PACIFIC NORTHWEST NATIONAL LABORATORY
operated by
BATTELLE
for the
UNITED STATES DEPARTMENT OF ENERGY
under Contract DE-AC05-76RL01830

Printed in the United States of America

Available to DOE and DOE contractors from
the Office of Scientific and Technical Information,
P.O. Box 62, Oak Ridge, TN 37831-0062

www.osti.gov

ph: (865) 576-8401

fox: (865) 576-5728

email: reports@osti.gov

Available to the public from the National Technical Information Service
5301 Shawnee Rd., Alexandria, VA 22312

ph: (800) 553-NTIS (6847)

or (703) 605-6000

email: info@ntis.gov

Online ordering: <http://www.ntis.gov>

Filtration of Hanford Tank 241-AW-105 Supernatant at 16 °C

May 2025

JR Allred
C Alvarez
AA Bachman
EC Buck
CA Burns
RC Daniel
JE Turner
RA Peterson

Prepared for
the U.S. Department of Energy
under Contract DE-AC05-76RL01830

Pacific Northwest National Laboratory
Richland, Washington 99354

Summary

Approximately 9 L of supernatant from Hanford waste tank 241-AW-105 was delivered by Washington River Protection Solutions (WRPS)¹ to the Radiochemical Processing Laboratory (RPL) at Pacific Northwest National Laboratory (PNNL). The thirty-six 241-AW-105 sample bottles consisted of four sets of nine samples, with each set pulled from a unique tank sampling level. Prior to testing, samples from each level were composited and diluted to 5.5 M Na to provide nominally level-independent feed for dead-end filtration and ion exchange testing.

The composited 241-AW-105 supernatant was chilled to 16 °C for 1 week prior to testing. Filtration testing was then conducted using a backpulse dead-end filter (BDEF) system equipped with a feed vessel and a Mott inline filter (Model 6610, Media Grade 5) in the hot cells of the RPL. The purpose of this testing was to (a) demonstrate dead-end filtration (DEF) of 241-AW-105 feed at reduced temperature to obtain prototypic Tank Side Cesium Removal (TSCR) flux rates and identify issues that may impact filtration after dilution to 5.5 M Na, and (b) provide feed for follow-on ion exchange unit operation.

The feed was filtered through the BDEF system at a targeted flux of 0.065 gpm/ft². For most of the filtration campaign, the differential pressure required to effect filtration at 0.065 gpm/ft² was slow to increase. After all the feed bottles had been pumped into the slurry reservoir, the bottoms of the bottles were added to the reservoir and transmembrane pressure (TMP) reached 2.0 psid (the TSCR action limit). A backpulse was performed after >50 hours of filtration to remove fouled solids and reduce the TMP. The filter was cleaned after completing filtration of the 241-AW-105 feed, and clean water flux tests showed filter performance was effectively restored.

Solids concentrated from the backpulse solutions were composed of steel-like particles, uranium-bearing phases, Mn-Fe phases, a Ce-bearing phase, Zr phases, and some smaller Ca-bearing particles. The Ca-bearing and U-bearing phases were identified as calcite and clarkeite, respectively.

¹ now Hanford Tank Waste Operations and Closure (H2C)

Acknowledgments

The authors gratefully acknowledge the help of hot cell technicians Victor Aguilar, Robert Cox, and Hollan Brown in conducting this work. We thank Renee Russell for conducting the technical review of this report. We also thank Matt Wilburn for technical editing of this report and David MacPherson for the quality reviews of the calculation packages and this report.

Microscopy work was performed at the Radiochemical Processing Laboratory Quiet-Suite at Pacific Northwest National Laboratory.

Acronyms and Abbreviations

AEA	alpha energy analysis
BDEF	backpulse dead-end filter (system)
BSE	backscatter electron
CWF	clean water flux
DEF	dead-end filtration
DOE	U.S. Department of Energy
EDS	X-ray energy dispersive spectroscopy
HAADF	high-angle annular dark-field
H2C	Hanford Tank Waste Operations and Closure
ICP-OES	inductively coupled plasma optical emission spectroscopy
IX	ion exchange
LAW	low-activity waste
MFC	mass flow controller
NQAP	Nuclear Quality Assurance Program
PNNL	Pacific Northwest National Laboratory
RPL	Radiochemical Processing Laboratory
SAED	selected area electron diffraction
SEM	scanning electron microscopy
STEM	scanning transmission electron microscopy
TEM	transmission electron microscopy
TMP	transmembrane pressure
TRU	transuranic
TSCR	Tank Side Cesium Removal
WRPS	Washington River Protection Solutions
WTP	Waste Treatment and Immobilization Plant
XRD	X-ray diffraction

Contents

Summary	ii
Acknowledgments.....	iii
Acronyms and Abbreviations	iv
Contents	v
1.0 Introduction.....	1.1
2.0 Quality Assurance.....	2.1
3.0 Test Conditions	3.1
3.1 BDEF Filtration	3.1
3.1.1 Backpulse Dead-End Filter System Description	3.1
3.1.2 System Operation during Testing.....	3.3
3.2 Feed Composite and Dilution	3.4
3.3 Feed Temperature Control.....	3.5
3.4 Sample Analysis	3.6
4.0 Results.....	4.1
4.1 Dilution Process Results	4.1
4.1.1 Clean Water Flux.....	4.1
4.2 Waste Filtering.....	4.2
4.3 Final CWF.....	4.8
4.4 Analytical Results.....	4.9
4.4.1 Diluted and Compositated AW-105 Supernatant Tank Waste Analysis	4.9
4.4.2 Total Alpha Analysis	4.10
4.4.3 Rheology Analysis of Filtered and Cesium Decontaminated AW-105 Supernatant Tank Waste.....	4.10
4.5 Alpha Energy Analysis	4.11
4.6 Microscopy Solids Analysis	4.11
4.6.1 SEM Analysis of AW-105 Solids-1, -2	4.12
4.6.2 Filtered Solution-1	4.15
4.6.3 Filtered Solution-3.....	4.19
5.0 Conclusions.....	5.1
6.0 References.....	6.1
Appendix A – BDEF Piping and Instrumentation Diagram	A.1
Appendix B – Feed Bottle Composite and Dilution	B.1
Appendix C – Total Alpha Analysis for Filtration Permeate Samples	C.1
Appendix D – ICP-OES Analysis for Diluted and Compositated 241-AW-105 Supernatant.....	D.1
Appendix E – Microscopy Analysis of Backpulsed Solids from AW-105.....	E.1
Appendix F – Alpha Energy Analysis of Backpulsed Solids from AW-105.....	F.1

Figures

Figure 3.1.	BDEF system installed in hot cell. HTX = heat exchanger.	3.2
Figure 3.2.	(a) Filter housing schematic (note that the 6610 series filter was welded to a 3/8-in. pipe fitting, making the configuration similar to the 6480 series illustrated here); (b) photo of modified filters with filter housings removed. (Mott 6480 line filter schematic from https://mottcorp.com .)	3.3
Figure 3.3.	AW-105 temperature in the trough heat exchanger.	3.6
Figure 3.4.	Concentrated solids after centrifuging in the hot cell (A: S1 solids, B: S2 solids, C: S3 solids) with 50-mL tubes.	3.7
Figure 3.5.	Concentrated solids in fume hood after centrifuging.	3.8
Figure 4.1.	CWF measurements for Media Grade 5 BDEF at 2.57 mL/min (0.065 gpm/ft ²) permeate rate (nominal) before testing. (Dashed line is average pressure over the 10-min period.).....	4.2
Figure 4.2.	Filter differential pressure and permeate flow rate during filtering operations.	4.4
Figure 4.3.	AW-105 filter resistance and permeate density during filtration process.	4.5
Figure 4.4.	Hermia blocking regimes modeled with AW-105 filtration resistance data leading up to the first backpulse.	4.8
Figure 4.5.	Initial and final CWF.	4.9
Figure 4.6.	SEM images of AW-105 Solids-1 sample.	4.13
Figure 4.7.	SEM image and EDS of Zr-hydroxide phase with a composition similar to that observed by Reynolds and co-workers (2014).....	4.13
Figure 4.8.	SEM images of AW-105 Solids-1 sample showing hematite particle agglomerate with a characteristic “rose-pellet” morphology.....	4.14
Figure 4.9.	SEM images of various particles and an identified uranium-bearing phase consistent with clarkeite in the AW-105 Solids-2 sample.	4.14
Figure 4.10.	SEM image and EDS maps of particle agglomerates found in the AW-105 Solids-1 sample showing NaF particles and zirconium phases.	4.15
Figure 4.11.	SEM images and EDS from particles observed in Filtered Solution-1. (A) Mn-Fe-phase, (B) cerium-bearing particle, and (C) steel particles.	4.16
Figure 4.12.	SEM and EDS analysis of a Mn-Fe and calcium particles associated with evaporated salt (that was not completely removed during sample preparation) from Filtered Solution-1.	4.17
Figure 4.13.	SEM images and EDS of uranium-bearing particles found in Filtered Solution-1.....	4.18
Figure 4.14.	Elemental map showing a Zr-bearing particle from Filtered Solution-1 together with Ca-bearing particles.	4.18
Figure 4.15.	Particles containing Zr from the Filtered Solution-1. Unclassified refers to particles that were not uniquely identified during the analysis. Over 1200 particle were analyzed.....	4.19
Figure 4.16.	SEM images of particles observed in Filtered Solution-3 with EDS analyses. (A) Ti-bearing particle, (B) Fe-Cr-steel particle, and (C) a uranium-bearing particle.	4.20
Figure 4.17.	SEM image with highlighted Cu-grid and EDS elemental maps of Filtered Solution-3 showing the occurrence of a few Si, Cr-Fe, and Mn particles but many Ca-bearing phases.	4.21

Figure 4.18. SEM image and EDS spectrum of a uranium-bearing particle in Filtered Solution-3..... 4.21

Figure 4.19. Particles containing Zr from the Filtered Solution-3. Over 3,000 particles were analyzed. The bright yellow in the figure represents the ‘unclassified’ particles. 4.22

Tables

Table 3.1.	Mass balance – BDEF.....	3.4
Table 3.2.	As-received samples.....	3.5
Table 3.3.	Backpulse concentrate samples.....	3.8
Table 4.1.	System timeline.....	4.3
Table 4.2.	Test parameters prior to backpulsing.	4.4
Table 4.3.	Post-filtration density measurements of product bottles.	4.6
Table 4.4.	Fouling period boundary points.	4.7
Table 4.5.	RMSE of resistance for each blocking regime model.....	4.8
Table 4.6.	ICP-OES results of diluted and composited AW-105 supernatant tank waste.	4.10
Table 4.7.	Total alpha analysis for permeate samples.....	4.10
Table 4.8.	Viscosity results of filtered and Cs decontaminated sample.....	4.11
Table 4.9.	AEA results for AW-105 solids: Measured alpha emitters, μCi per sample $\pm 1-\sigma$	4.11
Table 4.10.	Microscopy sample IDs.....	4.12
Table 4.11.	Sample analysis summary.	4.12

1.0 Introduction

The U.S. Department of Energy's Hanford Site houses 56 million gallons of highly radioactive tank waste generated from plutonium production from 1944 to 1988 (Gerber 1992). The supernatant waste, currently stored in underground tanks, is intended to be vitrified following filtration and ^{137}Cs removal at the Hanford Waste Treatment and Immobilization Plant (WTP) Pretreatment Facility. Because the Pretreatment Facility is not currently operational, ^{137}Cs will be removed from low-activity waste (LAW) vitrification feeds using the Tank Side Cesium Removal (TSCR) system, which will filter and then remove cesium from tank waste supernatant using ion exchange (IX) to support direct transfer of the TSCR-processed waste to the WTP LAW Facility. The TSCR system is skid-mounted and employs two key technologies: (1) dead-end filtration (DEF) for solids removal, which is necessary to protect the functionality of the IX columns, and (2) IX processing for cesium removal.

A small-scale test platform was established in 2017 to demonstrate these processes in the Radiological Processing Laboratory (RPL) at Pacific Northwest National Laboratory (PNNL).

Hanford waste tank 241-AW-105 (herein AW-105) is anticipated to be a future feed to TSCR. The purpose of this filtration testing was to (a) demonstrate DEF of an actual waste feed at reduced temperature (16 °C) to obtain prototypic TSCR flux rates and identify issues that may impact filtration and (b) provide feed for the IX unit operation (also part of the test platform). Approximately 9 L of AW-105 tank waste supernatant was delivered to PNNL in thirty-six 250-mL bottles. The thirty-six AW-105 sample bottles consisted of four sets of nine samples, with each set pulled from a unique depth within the tank supernatant layer. Prior to testing, samples from each level were composited and diluted to 5.5 M Na with process water sourced from the Columbia River to provide nominally level-independent feed for DEF and IX testing.

The AW-105 tank waste was filtered at reduced temperature (16 °C) to mimic the low end of temperatures that tank AW-105 can experience during the winter and spring months. Note that the AW-105 sample feed temperature was not controlled after the feed samples were collected from the Hanford Tank Operations Contractor and stored at the PNNL hot cell ambient temperature (~25 °C) from delivery until approximately 1 week prior to filtration at PNNL. The sodium content of the as-received AW-105 samples was expected to be ~5.9 M Na (Anderson 2024), and as such, AW-105 level-composites were diluted with Columbia River water to reduce their sodium molarity, as has been done in previous DEF and IX test campaigns (e.g., see Allred et al. 2023a, b).

The current filtration testing was conducted using a purpose-built backpulse dead-end filter (BDEF) system, which was designed to mimic filtration planned for use in the full-scale TSCR system. This equipment was used in fiscal years (FYs) 2020 through 2025 and is described in Allred et al. (2020).

2.0 Quality Assurance

This work was performed in accordance with the PNNL Nuclear Quality Assurance Program (NQAP). The NQAP complies with U.S. Department of Energy (DOE) Order 414.1D, *Quality Assurance*, and 10 CFR 830, Subpart A, *Quality Assurance Requirements*. The NQAP uses NQA-1-2012, *Quality Assurance Requirements for Nuclear Facility Applications*, as its consensus standard and NQA-1-2012, Subpart 4.2.1, as the basis for its graded approach to quality (ASME 2012).

The NQAP works in conjunction with PNNL's laboratory-level Quality Management Program, which is based on the requirements as defined in the DOE Order 414.1D, *Quality Assurance*, and 10 CFR 830, Subpart A, *Quality Assurance Requirements*.

The work described in this report was assigned the technology readiness level 5. All staff members contributing to the work received proper technical and quality assurance training prior to performing quality-affecting work.

3.0 Test Conditions

In October 2024, WRPS provided 36 supernatant samples (~250 mL each) from tank AW-105 in two batches. These samples were taken at four depths (39, 116, 194, 271 in. below the liquid surface level¹⁻²) in sets of nine – each set from a different depth – and provided to PNNL for filtration testing. At the RPL, the as-received AW-105 samples from each level were composited and diluted with process water sourced from the Columbia River to provide nominally level-independent feed with a sodium concentration of 5.5 M for filtration testing, which in turn would provide feed for IX and vitrification testing. The bottles of composited AW-105 tank waste were chilled (16 °C setpoint) for approximately 1 week prior to testing. Filtration testing of the tank waste used a Mott Model 6610 (Media Grade 5) sintered 316L stainless-steel line filter with a 0.317-in. porous diameter, 1.463-in. porous length, and 1.51-in.² filter area with porous end cap. Filtration testing of the AW-105 tank waste began on December 2, 2024.

3.1 BDEF Filtration

3.1.1 Backpulse Dead-End Filter System Description

AW-105 filtration was performed on the same BDEF system used in FY24 (Allred et al. 2024), again using the trough heat exchanger to keep all the feed at the setpoint temperature until it was added to the BDEF system. The feed bottles were stored in a trough heat exchanger with a cover, and feed was introduced into the BDEF system by removing a feed bottle from the trough just before pumping the waste contents into the slurry reservoir.

Once the feed was added to the BDEF slurry reservoir, it was continuously chilled at the setpoint temperature in a slurry recirculation loop via an in-line heat exchanger. In addition to maintaining slurry temperature, the recirculation loop kept the contents of the slurry reservoir well-mixed and provided nominally 20 psig of back pressure to drive the slurry through the filter. The filter was housed in a clamshell heat exchanger to maintain feed temperature as it entered and permeated the filter. The liquid permeate was no longer temperature-controlled downstream of the clamshell heat exchanger. A piping and instrumentation diagram is provided in Appendix A. Figure 3.1 shows a photograph of the BDEF system installed in the RPL Shielded Analytical Laboratory hot cell.

¹RPP-PLAN-66379, *Tank 241-AW 105 Large Volume Sample Collection to Support Platform Testing, Phase 1, FY24*

²RPP-PLAN-66402, *Tank 241-AW 105 Large Volume Sample Collection to Support Platform Testing, Phase 2, FY24.*

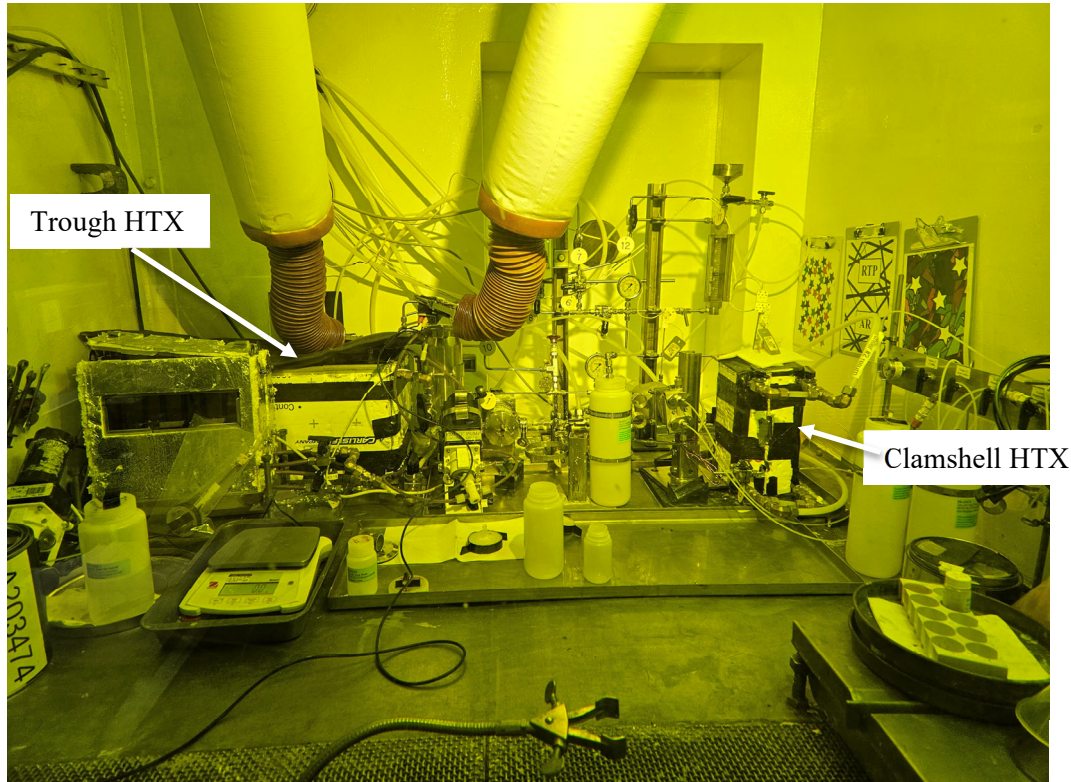


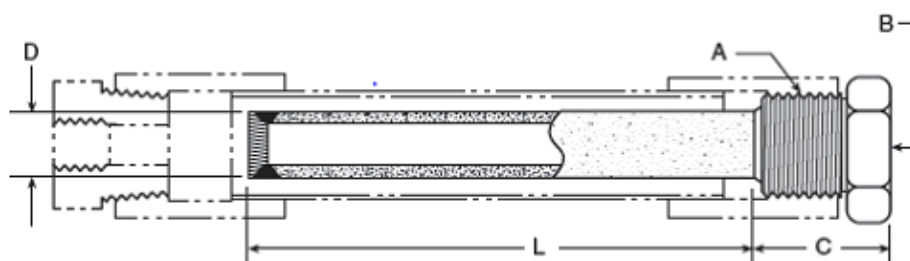
Figure 3.1. BDEF system installed in hot cell. HTX = heat exchanger.

The BDEF system is composed of a slurry recirculation loop, a filter assembly, and a permeate system. The main recirculation loop consists of a 1-L stainless-steel container (Eagle, EPV1A), a low-shear quaternary diaphragm pump (Quattro Flow QF150), a heat exchanger, and a throttle valve. The pump speed is controlled by a variable frequency drive located outside the hot cell. The slurry flow rate and pressure are controlled by adjusting the pump variable frequency drive (pump speed control) and throttle valve. The recirculation loop provides mixed, pressurized feed to the filter assembly. During the testing described in this report, the slurry temperature was controlled at a 16 °C setpoint.

The filter assembly receives pressurized slurry from the slurry recirculation loop. The filter assembly is composed of a filter, a Rosemount differential pressure transducer, and a flush valve (V3 in Appendix A). The flush valve is actuated during backpulse operations to clear solids off the filter and out of the system.

The permeate system receives permeate produced by the filter assembly. The permeate flow rate is controlled with a mass flow controller (MFC), which can control feed in the range of 0.15 to 0.33 L/h. These rates equate to allowable filter areas of 1.5 to 3.3 in.² assuming flux of 0.065 gpm/ft². The MFC also measures flow rate and density of the permeate, and a glass flowmeter is provided as a secondary flow rate measurement device. The permeate system can also perform a backpulse function, during which pressurized air is introduced into the backpulse chamber and used to force permeate (or other fluids) backward through the filter and out of the system.

The Mott 6610 filter used in testing is cylindrical, with dimensions of 0.317-in. diameter × 1.5-in. length and a filtration area of 1.51 in.². The filter element is fabricated from a seamless sintered stainless-steel tube that is a closed/dead-end porous tube (with a porous end cap); the open end is welded to a pipe-reducing bushing. At 0.065 gpm/ft², the rate of filter processing is 3.7 L of feed per 24-h day. Figure 3.2 shows a schematic of the filter assembly and a photo of the filter.



(a)

(b)

Figure 3.2. (a) Filter housing schematic (note that the 6610 series filter was welded to a 3/8-in. pipe fitting, making the configuration similar to the 6480 series illustrated here); (b) photo of modified filters with filter housings removed. (Mott 6480 line filter schematic from <https://mottcorp.com>.)

3.1.2 System Operation during Testing

The AW-105 waste samples were tested following the steps below:

1. **Compositing and dilution of AW-105 feed:** Four sampling sets of six bottles (~1.5 L of waste per set) were collected from unique sampling depths in tank AW-105. To provide level-independent feed for BDEF and IX testing, one sample bottle from each set was selected and the selected bottles were composited with one other to minimize set-to-set variation in physical/chemical properties. Eight separate composites of nominally 1 L of waste were created by combining one as-received bottle of waste from each sampling set into 1.5-L feed bottles. A ninth composite was created using three as-received bottles of waste from three of the sampling sets. (The fourth as-received bottle was set aside for the possibility of separate testing outside of the filtration and IX campaigns.) The composites were then diluted with sufficient process water sourced from the Columbia River to reduce the sodium molarity from 5.87 to 5.5 M Na. This process water was filtered through a Thermo Scientific 0.45 μ m asymmetric polyethersulfone (aPES) sterile disposable bottle top filter prior to use in dilution. Appendix B provides a detailed tabulation of how the 36 as-received sample jars were partitioned into the nine feed composite bottles. The diluted AW-105 feed was stored at the RPL hot cell ambient temperature (~25 °C) until 1 week before the filtration campaign began.
2. **Pre-testing temperature control:** Approximately 1 week prior to filtration, the composited and diluted AW-105 feeds were chilled to 16 °C and held at the reduced temperature until testing.
3. **Initial clean water flux (CWF):** The initial CWF measurement served as a system leak test and provided a baseline measurement of filter resistance. The measurement was conducted at nominal test conditions of 0.065 gpm/ft² with 0.01 M NaOH inhibited water for approximately 10 min.
4. **Filtration:** The 5.5 M Na AW-105 feed was filtered using a Mott Grade 5 sintered metal filter at a targeted flux of 0.065 gpm/ft². The targeted flux is based on the full-scale TSCR filter flux (5.0

gpm through 77 ft² of Mott sintered metal filter [0.065 gpm/ft²]¹. Filtration was performed at a targeted temperature of 16 °C. Filter resistance as a function of time was measured, and filter backflushing (“backpulsing”) was implemented when the filter differential pressure increased to 2 psi as per TSCR filter operation specifications¹. Backflush solutions were collected and analyzed.

5. **Permeate handling:** Permeate from testing was collected and retained for use as feed for subsequent IX testing. Temperature control (16 °C) of the filtered samples was maintained to the best extent practical, such that filtered permeates were returned to the trough after collection in any given bottle was complete.
6. **Filter cleaning:** The BDEF system was backpulsed and drained of all AW-105 before feeding 0.1 M NaOH through the system. The filter element was cleaned by soaking it in 0.1 M NaOH for a minimum of 2 h (prototypic of TSCR filter cleaning), followed by a filter backpulse using fresh 0.1 M NaOH. The system was then drained, rinsed and backpulsed with deionized water, and drained once more.
7. **Final CWF:** An additional CWF test was performed to ensure filter performance had been restored.
8. **BDEF system lay-up:** The system was rinsed, drained, and laid-up for storage.

Table 3.1 presents a mass balance for BDEF testing. A total of 12,238.6 g of AW-105 supernatant was added to the BDEF system during testing, and a total of 12,171.6 g was removed. The missing mass (~67.0 g) is due to evaporation and material that wets the inside of the BDEF system. It is not recoverable and represents less than 0.5% of the initial feed.

Table 3.1. Mass balance – BDEF.

Description	In (g)	Out (g)
Decanted supernatant filtration	12,238.6	--
Product to IX	--	12,009.6
Permeate samples	--	19.1
Backpulse samples	--	123.0
Drained from BDEF	--	21.8
Total	12,238.6	12,173.5

3.2 Feed Composite and Dilution

Tank waste supernatant was sampled from four unique liquid levels of tank AW-105, with nine 250-mL bottles received from each sample level for a total of 36 bottles. The samples were taken from tank liquid depths of 39, 116, 194, and 271 in. as shown in Table 3.2. Liquid properties such as viscosity, sodium molarity, and density can vary based on depth beneath the liquid surface due to stratification. A density measurement was taken from each of the sampling groups prior to the compositing process. Of the 36 as-received bottles, 35 were composited and diluted and one was set aside for a separate study outside the scope of the filtration campaign. Four receipt bottles from four different sampling locations were combined into individual 1.5-L filtration feed bottles, producing 8 feed bottles containing ~1.1 L of composited waste. A ninth bottle was prepared with three receipt bottles from three different sampling locations. Process water sourced from the Columbia River – a practice used in TSCR – was then added to each filtration feed bottle to dilute the wastes from ~5.87 M (Anderson 2024) to nominally 5.5 M Na. Appendix B provides details on the diluted bottle compositions.

¹ RPP-CALC-62496, Rev. 03, *TSCR Filter Sizing*.

Table 3.2. As-received samples.

Sample Location (depth below liquid surface, in.)	Receipt Sample Jar ID			Density (g/mL)
39	5AW-24-01	5AW-24-02	5AW-24-03	1.300
	5AW-24-04	5AW-24-05	5AW-24-06	
	5AW-24-07	5AW-24-08	5AW-24-09	
116	5AW-24-10	5AW-24-11	5AW-24-12	1.303
	5AW-24-13	5AW-24-14	5AW-24-15	
	5AW-24-16	5AW-24-17	5AW-24-18	
194	5AW-24-19	5AW-24-20	5AW-24-21	1.300
	5AW-24-22	5AW-24-23	5AW-24-24	
	5AW-24-25	5AW-24-26	5AW-24-27	
271	5AW-24-28	5AW-24-29	5AW-24-30	1.302
	5AW-24-31	5AW-24-32	5AW-24-33	
	5AW-24-34	5AW-24-35	5AW-24-36	

3.3 Feed Temperature Control

The diluted AW-105 supernatant was chilled at a 16 °C setpoint temperature beginning on 11/25/2024 to provide adequate time (7 d) for the filtration feed to reach the processing temperature of 16 °C ± 2.2 °C. Daily temperature checks were performed on the feed to monitor cooling.

Figure 3.3 shows the temperature profiles recorded by various temperature elements throughout the filtration test. The slurry recirculation loop temperature (TE-101) was recorded using a thermocouple on the recirculation loop, and the filter inlet and outlet temperatures (TE-102 and TE-103, respectively) were recorded using resistance temperature detectors on the inlet and outlet lines of the filter. The trough temperature (TE-104) was recorded using a 12-in. resistance temperature detector affixed to the lid of a feed bottle so the probe would remain in contact with the liquid in the bottle throughout testing.

The slurry recirculation loop, filter inlet line, filter outlet line, and trough temperatures were maintained within the prescribed range of 16 °C ± 2.2 °C throughout filtration. The trough temperature probe recorded two spikes in temperature – one on 12/02/24 and one on 12/04/24 – which were aligned with recorded movements of TE-104 between feed bottles as they were queued to be fed into the BDEF system. An outlier was also recorded by the slurry recirculation loop on 12/04/2024, which coincided with a backpulse during which slurry recirculation was paused.

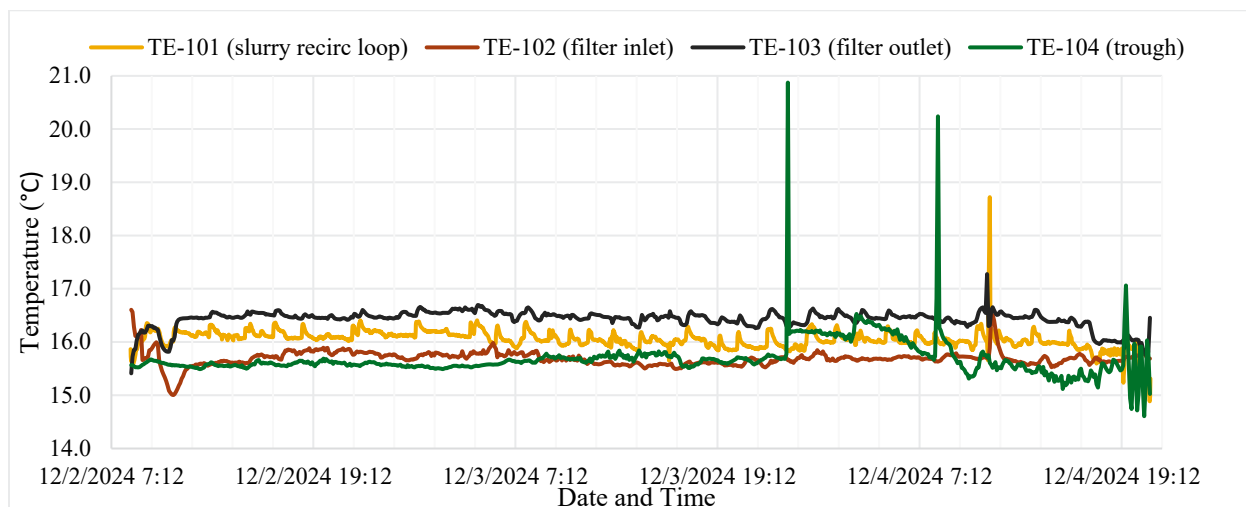


Figure 3.3. AW-105 temperature in the trough heat exchanger.

3.4 Sample Analysis

Three permeate samples (TI-177-P1, TI-177-P2, TI-177-P3) were collected after approximately one-third, two-thirds, and all the AW-105 feed had been filtered. These samples were submitted for total alpha analysis to determine the transuranic (TRU) content of the filtered permeate.

Backpulse concentrates were retained and kept separate (TI-177-S1, TI-177-S2, TI-177-S3, TI-177-S4). Upon completion of filtration testing, the solids were concentrated as shown in Figure 3.4.

To concentrate solids, backpulse solutions collected were centrifuged at 2,250 rpm for 15 min. The centrifuge had a rotor radius of 10 cm, resulting in a relative centrifugal force of 566 g. Due to the large volume of solution collected during backpulsing, some samples were split into two smaller subsamples prior to centrifuging. The bulk amount of the supernatant was then decanted and the solids from the samples that were split were resuspended and combined. The concentrated solutions were centrifuged once more at 2,250 rpm for 15 min. More supernatant was removed, and the solids were resuspended and transferred to clean centrifuge tubes for removal from the hot cell.

Once removed from the hot cell, the TI-177-S1 (S1) and TI-177-S3 (S3) concentrated solutions were segregated for solids washing while the TI-177-S2 (S2) sample was sent for alpha energy analysis as outlined in Table 3.3. The S1 and S3 samples were transferred to the smaller 15-mL centrifuge tubes and the solids were spun down for 15 min at 2,500 rpm. This centrifuge had a rotor radius of 14.4 cm, resulting in a relative centrifugal force of 1,006 g. Additional supernatant was removed to reduce the dose of the sample prior to sending it to the microscopy staff. These samples were then washed with a simple simulant containing 1.6 M NaOH and 3.9 M NaNO₃ in deionized water to further reduce sample dose by washing/diluting supernate liquid from the solids. Figure 3.5 shows the solids that were collected from the backpulsed solution after centrifuge, decant, and wash iterations.

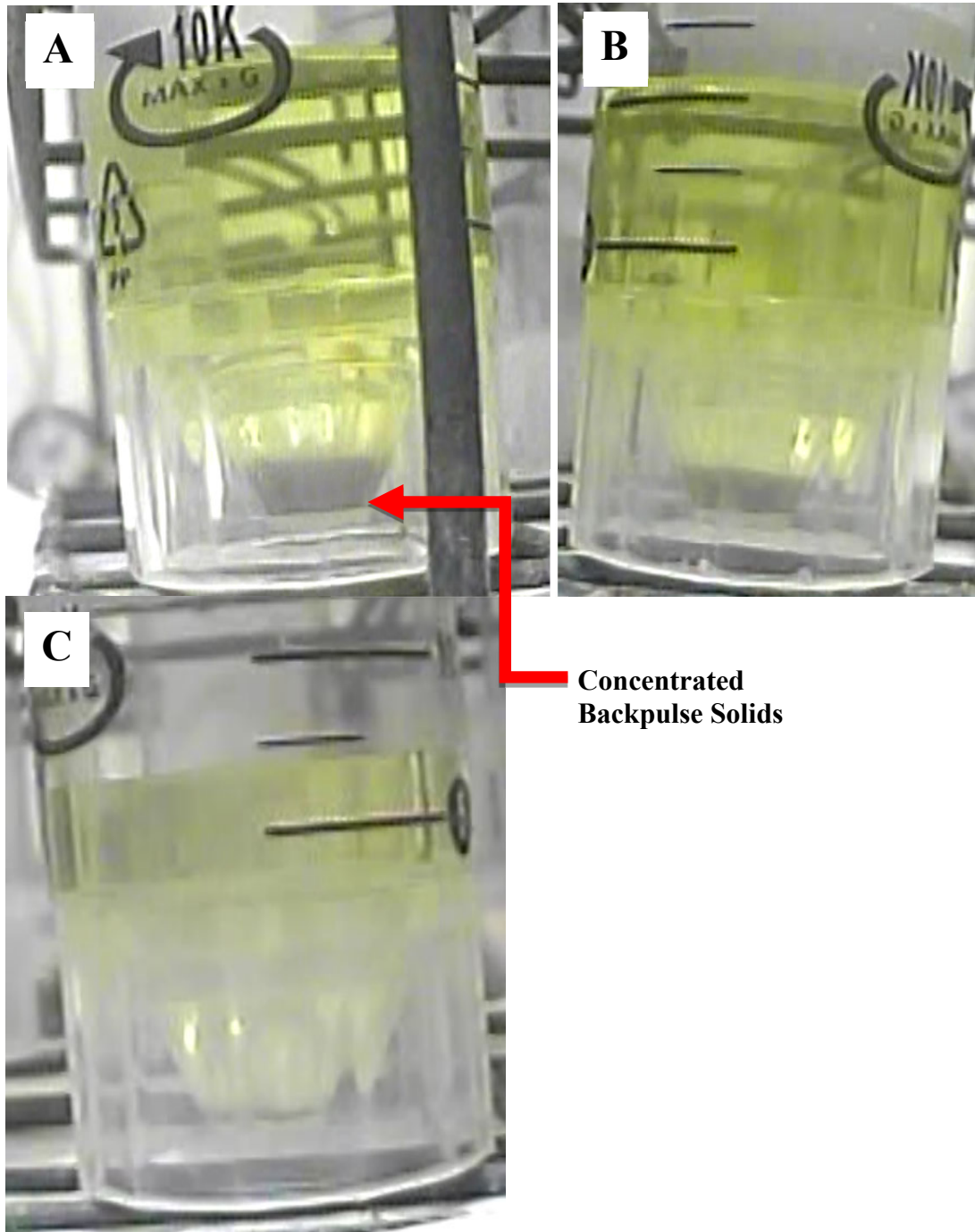


Figure 3.4. Concentrated solids after centrifuging in the hot cell (A: S1 solids, B: S2 solids, C: S3 solids) with 50-mL tubes.

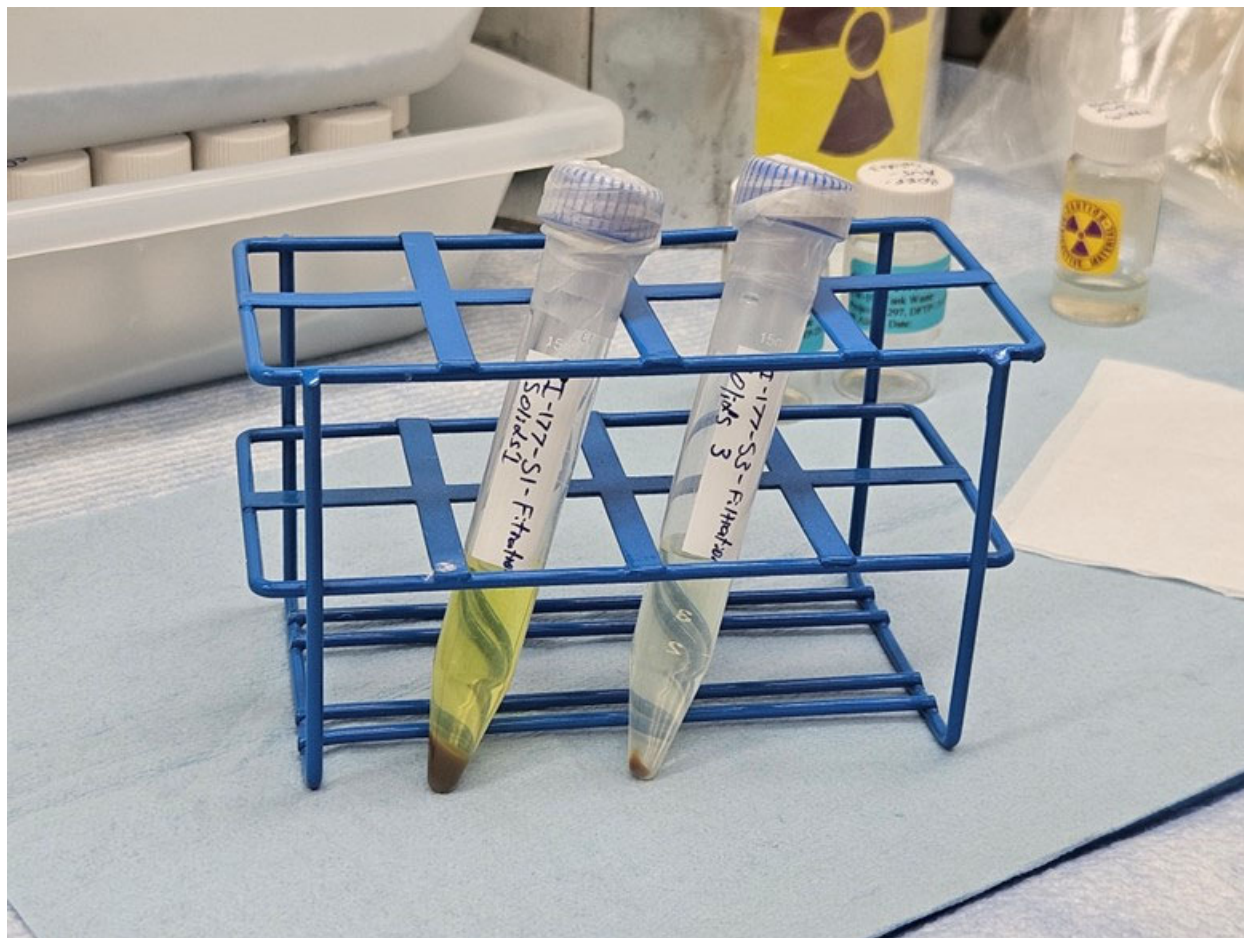


Figure 3.5. Concentrated solids in fume hood after centrifuging.

Table 3.3. Backpulse concentrate samples.

Sample ID	Contents	Analysis to be Performed on Solids
TI-177-S1	AW-105 solids concentrate from first backpulse (during filtration testing to reduce TMP)	Microscopy
TI-177-S2	AW-105 solids concentrate from second backpulse (at the end of filtration testing before draining the system)	Alpha energy analysis
TI-177-S3	0.1 M NaOH filter cleaning backpulse concentrate with AW-105 residue	Microscopy
TI-177-S4	0.01 M NaOH CWF backpulse concentrate	None

4.0 Results

4.1 Dilution Process Results

The density of a sample taken from composited and diluted bottle BDEF-AW5-1 was measured using a 10-mL Class A volumetric flask and an analytical balance. The measured density was 1.278 g/mL at an ambient cell temperature of 23.7 °C. Inductively coupled plasma-optical emission spectroscopy (ICP-OES) results of post-filtration samples showed an average Na concentration of 5.53 M Na.

4.1.1 Clean Water Flux

The objective of the CWF was to assess the state of the system at the start of testing to ensure a uniform basis for comparing different filtration trials, and to ensure that the system was “clean” at the start of testing. Figure 4.1 shows the initial CWF at 16.0 °C using 0.01 M NaOH with the Media Grade 5 stainless-steel BDEF filter. The CWF tests were conducted at ambient cell temperature at a nominal permeate flow rate of 2.57 mL/min (0.065 gpm/ft²). The transmembrane pressure (TMP) averaged 0.127 psid in the initial CWF with an average filter resistance of $1.80 \times 10^{10} \text{ m}^{-1}$. Resistance, $R \text{ [m}^{-1}\text{]}$, is calculated via Darcy’s law:

$$Q = \frac{PA_t}{\mu R} \quad (4.1)$$

where Q is the volumetric flow rate [m^3/s], P is the TMP [Pa], A_t is the total filter area [m^2] [$9.74 \times 10^{-4} \text{ m}^2$], and μ is the filtrate dynamic viscosity [$\text{Pa}\cdot\text{s}$] (4.887 mPa s, as measured at 16.0 °C – see Section 4.4.3 for additional details). For the present use, Eq. (4.1) is rearranged to allow calculation of filter resistance by

$$R(t) = \frac{P(t)A_t}{\mu Q(t)} \quad (4.2)$$

Prior CWF results on the BDEF system with this filter ranged from 0.015 to 0.2 psid TMP (Allred et al. 2024). These values all are likely within the accuracy of the CWF measurement and represent a relatively clean filter. Estimates of the resistance for the Mott 6610 series Grade 5 filter are $\sim 2 \times 10^{10} \text{ m}^{-1}$. The average TMP of 0.121 psid (shown in Figure 4.1) during the CWF indicates a lack of fouling on the filter (due to residual solids in the system). As such, these results indicate an overall clean system at the start of testing.

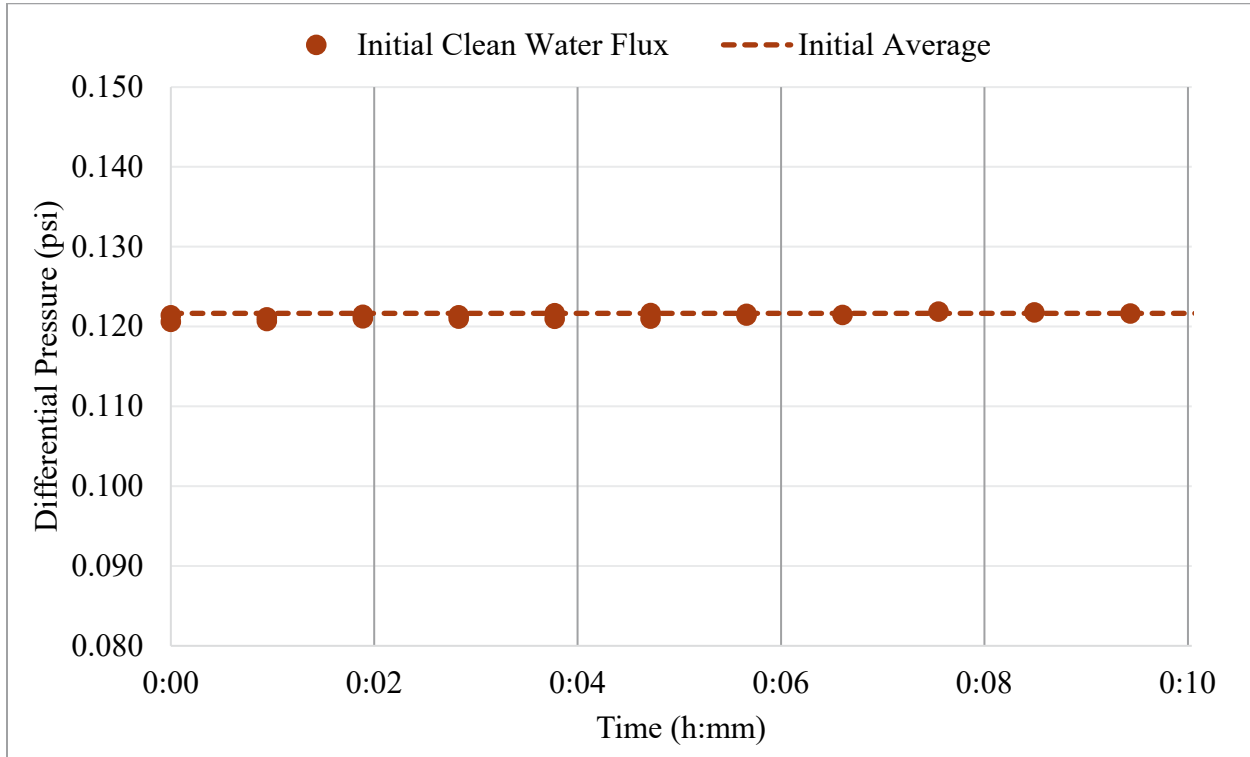


Figure 4.1. CWF measurements for Media Grade 5 BDEF at 2.57 mL/min (0.065 gpm/ft²) permeate rate (nominal) before testing. (Dashed line is average pressure over the 10-min period.)

4.2 Waste Filtering

When evaluating time rate changes in filter resistance and TMP during constant flow rate filtration, filtration behavior is generally evaluated against the specific volume filtered $v(t)$, which is simply the total volume filtered over a given filtration period normalized to the filter area, namely

$$v(t) = \frac{1}{A_t} \int_{t=0}^t Q(\tau) d\tau \quad (4.3)$$

In the present analysis, Eq. (4.4) references $t = 0$ to the start of filtration. Events throughout the filtration test can be described with respect to the total volume filtered per filter area in m³/m² rather than time elapsed since the start of filtration via Eq. (4.4).

BDEF feed bottles were stored in the trough heat exchanger to maintain feed temperature control at 16 ± 2.2 °C starting 1 week prior to filtration testing. AW-105 was transferred via a metering pump from each feed bottle in sequential order into the BDEF reservoir until approximately 2 in. of feed solution remained in the feed bottle. The remaining “bottoms” from each feed bottle were consolidated and fed into the system after all feed bottles had been reduced to 2 in. of remaining feed. The filtration rate was controlled by a MFC set to a permeate flow rate of 2.57 mL/min (0.065 gpm/ft²). Slurry recirculation line pressure was kept between 20 and 25 psi with adjustments to recirculation backpressure to correct for pressure deviations outside this range. One backpulse was performed during filtration testing while consolidated bottoms were being filtered after 8.3 m³/m² of waste had been filtered (~51 h after the start of filtration). Table 4.1 provides a timeline for the filtration testing, indicating feed bottle change, permeate bottle change, and process liquid flow.

Table 4.1. System timeline.

Date	Time	Volume Filtered (m ³ /m ²)	Event
2-Dec	8:20	0.00	Filtration started with BDEF-AW5-1, dewatering into IX-AW5-1
	9:12	0.14	Started pumping in BDEF-AW5-2
	15:25	1.12	Pumping from BDEF-AW5-3
	16:41	1.32	Product bottle switch to IX-AW5-2
	21:50	2.13	Feed bottle change to BDEF-AW5-4
3-Dec	1:07	2.65	Product bottle switch to IX-AW5-3
	4:44	3.22	Feed bottle change to BDEF-AW5-5
	8:16	3.78	Product bottle switch to IX-AW5-4
	8:20	3.79	24 hours running time
	9:20	3.95	Feed bottle change to BDEF-AW5-6
	15:31	4.93	Product bottle switch to IX-AW5-5
	16:16	5.05	MFC cable bumped and needed to be reseated
	17:19	5.20	Feed bottle change to BDEF-AW5-7
	23:24	6.16	TE-104 moved to BDEF-AW5-9
	23:35	6.20	Product bottle switch to IX-AW5-6
4-Dec	0:27	6.33	Feed bottle change to BDEF-AW5-8
	3:20	6.79	TE-104 moved to BDEF-AW5-9
	3:35	6.83	Feed bottle change to BDEF-AW5-9
	7:14	7.40	Product bottle switch to IX-AW5-7
	8:19	7.57	TE-104 moved to BDEF-AW5-1 (consolidated bottoms bottle)
	8:20	7.57	48 hours running time
	10:31	7.92	Feed bottle change to BDEF-AW5-1 (consolidated bottoms bottle)
	11:11	8.02	Differential pressure reached 2.0 psid, preparing for backpulse
	11:22	8.03	Backpulsed into TI-177-S1
	15:17	8.63	Product bottle switch to IX-AW5-8
19:11	9.25	Backpulse chamber filled from slurry reservoir	
19:23	9.27	Heel of BDEF-AW5-1 (consolidated bottoms bottle) poured into slurry reservoir	
20:54	9.51	Recirculation pump off; filtration test complete	

Testing began on the morning of December 2, 2024. Figure 4.2 shows TMP increased slowly from 0.215 psid until it reached 0.246 psid at 1.12 m³/m², when the feed bottle was switched to BDEF-AW5-3. A noticeable rate increase in TMP was observed between 1.12 and 6.33 m³/m². Then another noticeable rate increase in TMP was observed at 6.33 m³/m², when the feed bottle was switched to BDEF-AW5-8.

TMP then increased steadily to 1.485 psid at 7.92 m³/m² before TMP began to increase significantly faster, coinciding with the first introduction of consolidated bottoms into the feed. TMP reached the 2-psid limit at 8.02 m³/m², and a backpulse was performed. Table 4.2 presents the system parameters prior to backpulse.

Table 4.2. Test parameters prior to backpulsing.

Test Event	Volume Filtered (m ³ /m ²)	Filtration Resistance(1/m)	Transmembrane Pressure (psid)
Backpulse	6.39×10 ¹⁰	8.02	2.07

The initial backpulse reduced the TMP to ~0.22 psid. Differential pressure increased slowly and never exceeded 0.30 psid for the remainder of the test. The BDEF testing was declared complete at 9.51 m³/m². The momentary pressure spike seen in Figure 4.2 at 9.27 m³/m² occurred while the backpulse chamber was being filled in preparation for exhausting the feed.

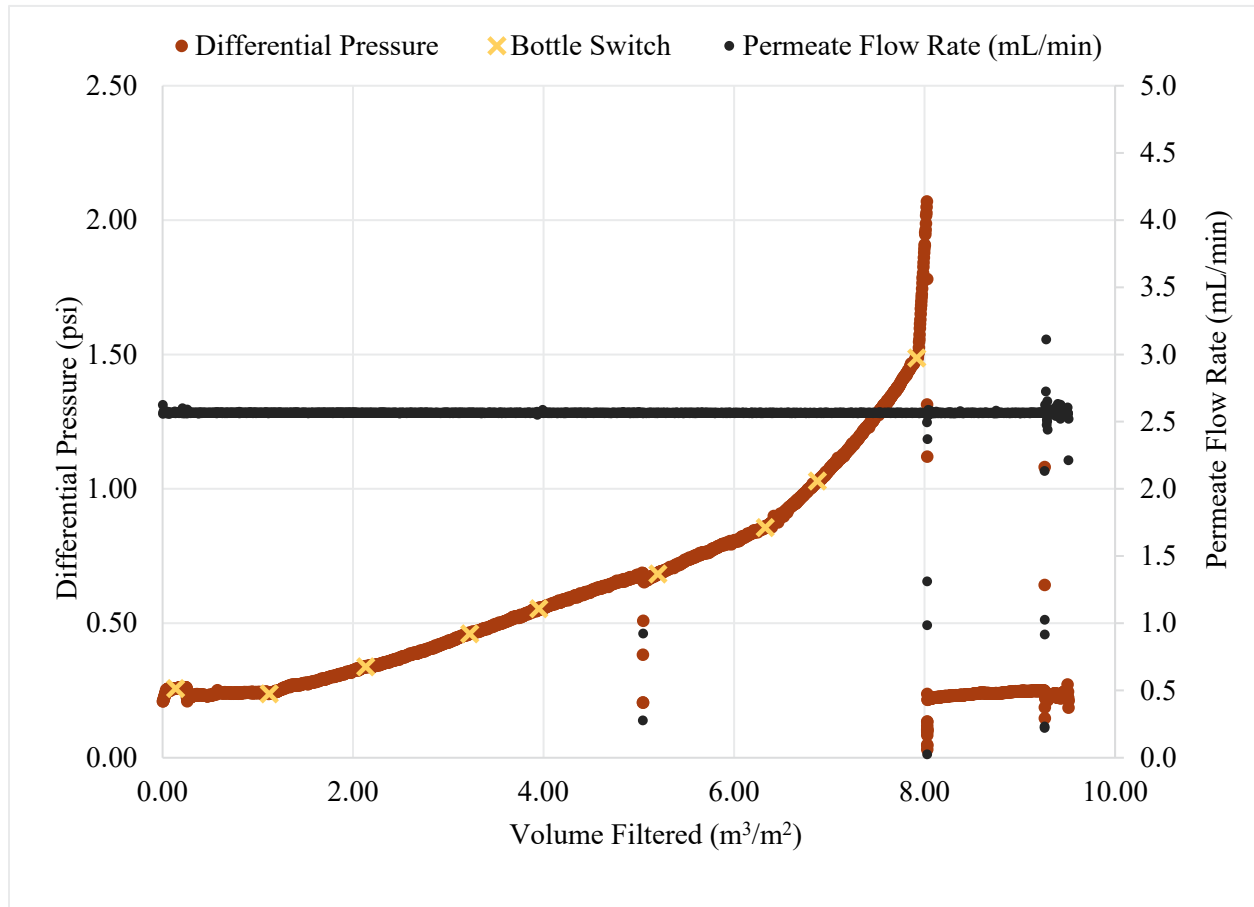


Figure 4.2. Filter differential pressure and permeate flow rate during filtering operations.

Figure 4.3 shows both the total filter resistance and the permeate density as a function of volume filtered over the 3 days of testing. Filter resistance was nominally constant until 1.12 m³/m², when the feed bottle was switched to BDEF-AW5-3. Filter fouling was then observed at a steady rate until 7.92 m³/m², when the feed bottle was switched to the consolidated bottoms. A small and steady increase in resistance was observed after backpulsing at 8.02 m³/m². Fouling of the filter by waste particulates, and the time rate change of filter resistance with volume filtered, provides information on the underlying fouling mechanism, which is expanded on later in this section.

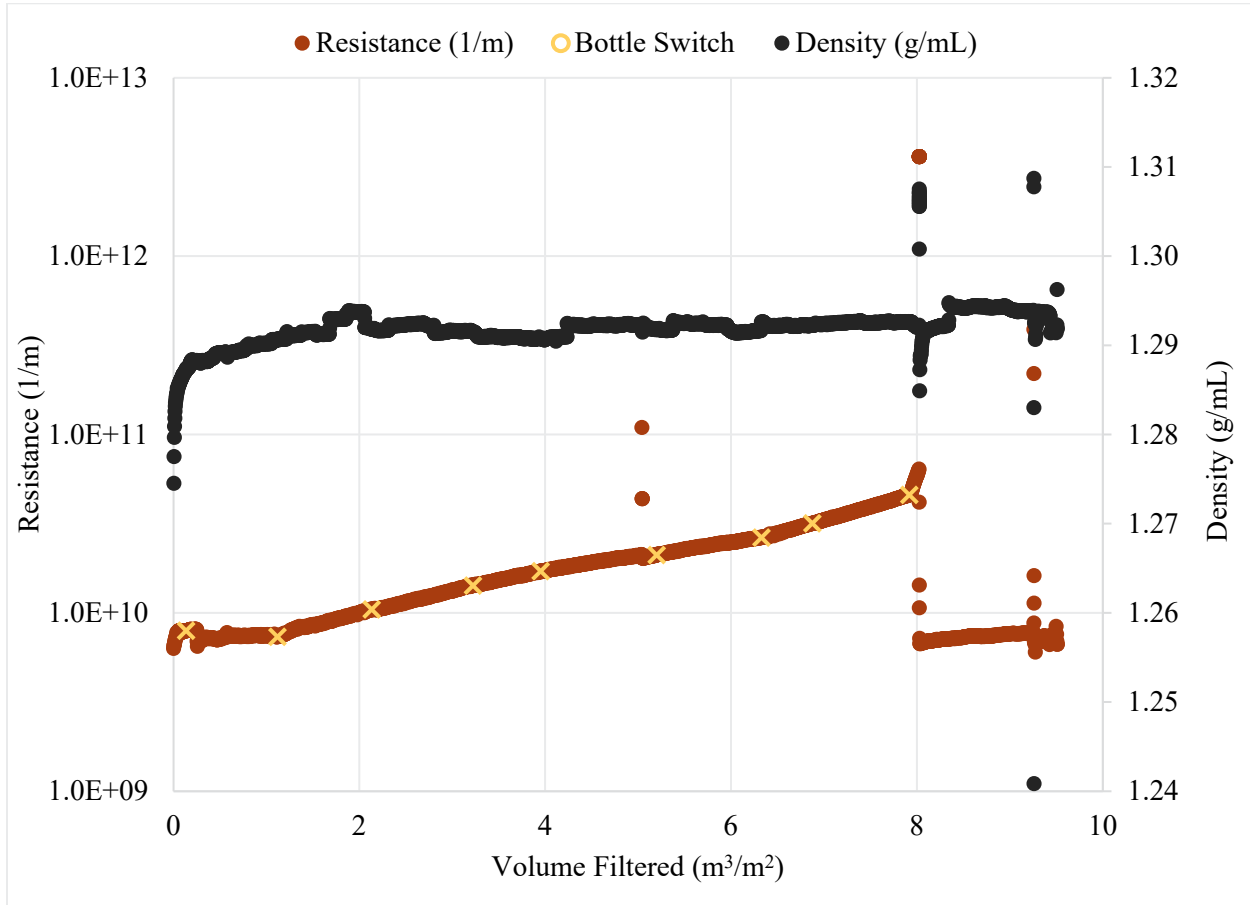


Figure 4.3. AW-105 filter resistance and permeate density during filtration process.

The density of the diluted and composited AW-105 solution nominally ranged between 1.285 and 1.295 g/mL per the MFC as shown in Figure 4.3 and averaged 1.290 g/mL through testing. The addition of the feed bottoms at 7.92 m³/m² did not induce any related density spikes.

Post-filtration analysis of the product bottles prior to IX included measuring product density in a 10-mL volumetric flask at 23.0 °C. The results are reported in Table 4.3 and show little variation in density between bottles. Average bottle density was 1.2804 g/mL with a standard deviation of 0.0019 g/mL and percent relative standard deviation of 0.15%.

Table 4.3. Post-filtration density measurements of product bottles.

Bottle ID	Density (g/mL)
IX-AW5-1	1.2768
IX-AW5-2	1.2806
IX-AW5-3	1.2798
IX-AW5-4	1.2807
IX-AW5-5	1.2797
IX-AW5-6	1.2803
IX-AW5-7	1.2826
IX-AW5-8	1.2827

The nature of potential particle-filter interactions occurring during transient increases in filter resistance can be characterized using fouling models proposed by Hermia (1982). A generic form of Hermia's model defines the resistance coefficient:

$$\frac{d^2t}{dV^2} = k_n \left(\frac{dt}{dV}\right)^n \quad (4.4)$$

Here, k_n and n are both constants dependent on the fluid properties and filter blocking regime, and V is the volume of permeate at t . Given the volumetric flow rate $Q = \frac{dV}{dt}$, the filter flow rate form of Hermia's model is

$$\frac{dQ}{dV} = -k_n Q^{2-n} \quad (4.5)$$

For a reduced resistance defined by $\omega = \frac{R}{R_0}$, where R is the filter resistance and R_0 is the initial filter resistance at the start of a filtration period, the reduced resistance can be described by the differential equation:

$$\frac{d\omega}{d\nu} = \kappa_n \omega^n \quad (4.6)$$

with

$$\kappa_n = \left(\frac{A_0}{Q_0^{n-1}}\right) k_n \quad (4.7)$$

where ν is the volume filtered per unit filter area, Q_0 is the initial volumetric flow rate for a filtration period, and A_0 is the initial permeable area of the filter prior to fouling of the same filtration period. By integrating Eq. (4.5),

$$\int_{\omega_0}^{\omega} \frac{d\omega}{\kappa_n \omega^n} = \int_{\nu_0}^{\nu_f} d\nu \quad (4.8)$$

the reduced resistance can be modeled when $n \neq 1$ by

$$\omega = [\omega_0^{1-n} + (1 - n)\kappa(v - v_0)]^{\frac{1}{1-n}} \quad (4.9)$$

with

$$\kappa = \frac{\omega_f^{1-n} - \omega_0^{1-n}}{(v_f - v_0)(1 - n)} \quad (4.10)$$

or when $n = 1$ by

$$\omega = \omega_0 e^{\kappa(v - v_0)} \quad (4.11)$$

with

$$\kappa = \left(\frac{1}{v_f - v_0} \right) \ln \frac{\omega_f}{\omega_0} \quad (4.12)$$

Hermia defined four blocking regimes with corresponding values of n :

- Cake filtration ($n = 0$)
- Intermediate blocking ($n = 1$)
- Standard blocking ($n = 1.5$)
- Pore (complete) blocking ($n = 2$)

Hermia's blocking regimes can be modeled using AW-105 filtration data from the fouling period presented in Table 4.4. The upper bound of the volume filtered, $v_f = 7.92 \text{ m}^3/\text{m}^2$, marks the initial introduction of consolidated bottoms into the feed reservoir, and the measured resistance that followed was excluded from the model due to its abruptness and short-lived change in fouling behavior prior to backpulsing. Figure 4.4 plots the resulting models of the four blocking regimes applied to the AW-105 filtration data with the actual AW-105 filtration resistance.

Table 4.4. Fouling period boundary points.

	Date/Time	Volume Filtered per Unit Filter Area (m^3/m^2)	Resistance (m^{-1})
Start	12/2/2024 8:21 AM	0.00	5.22E9
End	12/4/2024 10:32 AM	7.92	3.80E10

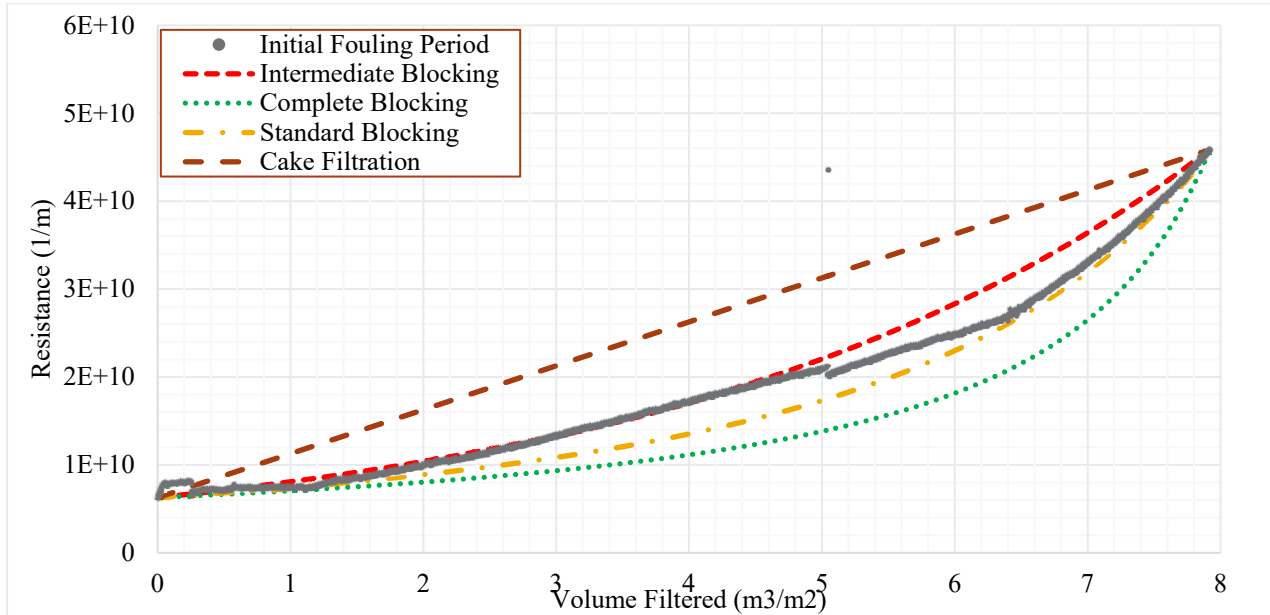


Figure 4.4. Hermia blocking regimes modeled with AW-105 filtration resistance data leading up to the first backpulse.

Visual interpretation of the models compared to the resistance data shows that both intermediate and standard blocking models coincide significantly with the AW-105 filtration resistance data. The root mean square error (RMSE) between the actual resistance data and the modeled resistance data is used to quantify the accuracy of each model in Table 4.5. The intermediate blocking model showed the lowest RMSE of 2.63E+09. The RMSE of the standard blocking model was 2.88E+09 – only 9.51% larger than the RMSE of the intermediate blocking model, suggesting characteristic fouling behavior of both intermediate and standard blocking mechanisms are prevalent when filtering AW-105 supernatant with the Mott stainless-steel Grade 5 filter.

Table 4.5. RMSE of resistance for each blocking regime model.

Regime	Blocking Exponent n	RMSE (m ⁻¹)
Cake Filtration	0	8.24E+09
Intermediate Blocking	1	2.63E+09
Standard Blocking	1.5	2.88E+09
Complete Blocking	2	5.29E+09

4.3 Final CWF

At the conclusion of AW-105 filtration, a filter cleaning evolution was initiated to precede the final CWF. A CWF at 16.1 °C was measured following filter cleaning, producing a differential pressure averaging 0.120 psid – while the initial CWF TMP was 0.121 psid as shown in Figure 4.5. This indicates that the 0.1 M NaOH filter cleaning protocol successfully restored membrane performance to pre-test conditions.

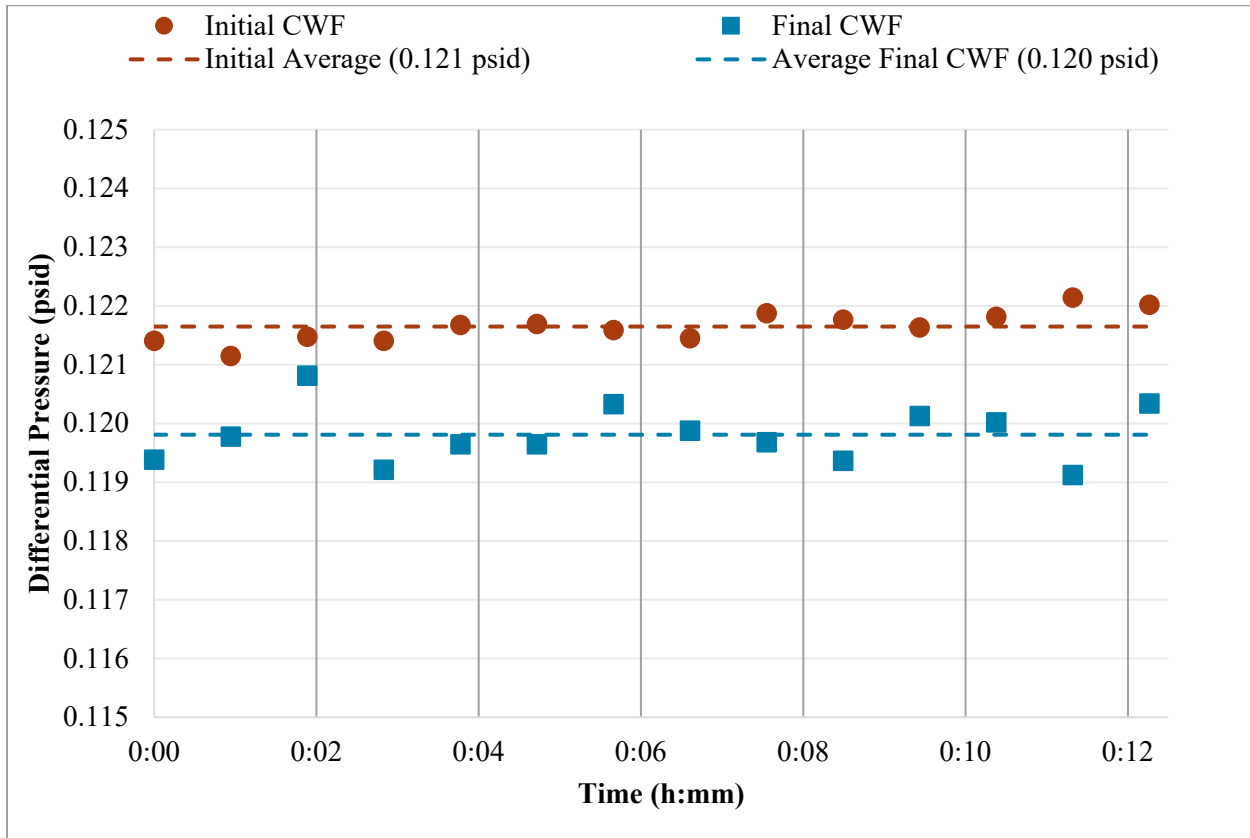


Figure 4.5. Initial and final CWF.

4.4 Analytical Results

4.4.1 Diluted and Composited AW-105 Supernatant Tank Waste Analysis

ICP-OES analysis was conducted on the diluted and composited AW-105 supernatant tank waste on a mass-per-unit-mass basis ($\mu\text{g/g}$) as presented in Table 4.6. Subsequently, the molarity of the diluted and composited waste was calculated using a density of 1.254 g/mL, which was determined after sample dilution and composite completion of the AW-105 tank waste. The detailed ICP-OES report is found in Appendix D.

The molarity was calculated using the following equation:

$$M = \frac{(m * \rho)}{MW} \quad (4.13)$$

where M is the molarity, m is the mass, ρ is the density, and MW is the molecular weight of the component.

Table 4.6. ICP-OES results of diluted and composited AW-105 supernatant tank waste.

Analysis Method	Analyte	Concentration ($\mu\text{g/g}$)	Molarity (mol/L)
ICP-OES	Na	102,938	5.72

4.4.2 Total Alpha Analysis

Total alpha analysis was conducted to determine the TRU content of the filtered permeate. The analysis results are given in Table 4.7 and show no gross breakthrough of TRU components that are not already soluble. Additional detail is provided in Appendix C. All samples were below the 0.1 $\mu\text{Ci/g}$ threshold defining TRU waste per DOE M 435.1-1, *Radioactive Waste Management Manual*.

Table 4.7. Total alpha analysis for permeate samples.

Analysis Method	Sample ID	IX Product Bottle Sampled From	($\mu\text{Ci/mL}$)	($\mu\text{Ci/g}$)
Total alpha analysis	TI-177-P1	IX-AW5-1	2.68E-4	2.06E-4
	TI-177-P2	IX-AW5-5	5.58E-5	4.29E-5
	TI-177-P3	IX-AW5-8	9.80E-5	7.53E-5

4.4.3 Rheology Analysis of Filtered and Cesium Decontaminated AW-105 Supernatant Tank Waste

The viscosity of the filtered and cesium-exchanged AW-105 supernatant was measured with a Haake M5-RV20 (equipped with an M5 measuring head and RC20 controller) and an MV1 rotor and cup measuring system. Temperature was controlled using a water jacket and a PolyScience refrigerated circulator, Model Number SD07R-20-A11B. This circulator allows heating and cooling of recirculation fluid to the water jacket over a range of -20 to 170 °C with a stability of ± 0.04 °C. Performance checks using a Cannon-certified viscosity reference standard, N10, (Cannon Instrument Company) were carried out prior to and after measurements to verify that the system was functioning as expected. Viscosity was measured using a standard flow curve protocol comprising an up-ramp from 0 to 1,000 s^{-1} for 5 min, a hold of 60 s at 1000 s^{-1} , and finally a down-ramp from 1,000 to 0 s^{-1} over 5 min. Flow curves were measured at four temperatures: 10, 16, 25, and 35 °C. For each temperature, the Newtonian viscosity¹ of the liquid was determined by linear regression of the down-ramp data. The fit range at each temperature was selected to exclude data impacted by the onset of secondary flows (i.e., Taylor vortices). The results of linear regression analysis and the resulting best fit Newtonian viscosities are reported in Table 4.8. The measured viscosity of the AW-105 supernatant is below the recommended range of the measuring system (nominally 5.5 to 650 mPa s) for both the 25 and 35 °C flow curves.

¹ While the AW-105 supernatant is expected to be Newtonian, linear regression analysis allowed for non-zero intercept to accommodate a non-zero torque offset introduced by the operator to accommodate negative torques resulting from operating the M5 viscometer outside its standard operating range (in this case, for viscosities below 5.5 mPa s).

Table 4.8. Viscosity results of filtered and Cs decontaminated sample.

Temperature (°C)	Fit Range	Viscosity	
	Down-Ramp, s ⁻¹	mPa s	Uncertainty ^(a) 3-Sigma Relative % Standard Error
10	50-1,000	6.321	1.013
16	50-1,000	5.095	0.952
25	50-650	3.619	3.274
35	50-550	2.840	4.752

(a) The uncertainty reported by the Haake software for the curve fit is the 3-sigma relative percent standard error.

4.5 Alpha Energy Analysis

Alpha energy analysis (AEA) was performed on the solids concentrated from the second backpulse as outlined in Table 4.9. The solids were dried down to measure an accurate mass. A Pu-242 and Am-243 tracer was added, and the sample was then digested in Optima-grade HNO₃. Additional detail is provided in Appendix F.

Table 4.9. AEA results for AW-105 solids: Measured alpha emitters, μCi per sample ± 1-σ.

Sample	Am-241	Pu-239 + 240	Pu-238
TI-177-S2 (BDEF-AW5-Solids 2)	2.45E-02 ± 2%	4.11E-03 ± 2%	1.80E-03 ± 2%
TI-177-S2 Duplicate	2.45E-02 ± 2%	4.14E-03 ± 2%	1.78E-03 ± 2%
Relative Percent Difference	0%	1.12%	0.73%

4.6 Microscopy Solids Analysis

Material collected from the concentrated backpulse solution was submitted for microscopy examination. Additional AW-105 solids supplied from the 222-S laboratory were also analyzed to provide additional context for the supernate solids. These solids were initially characterized in Ritenour (2006). The solids from the received AW-105 samples were identified using scanning electron microscopy (SEM) and X-ray energy dispersive spectroscopy (EDS) mapping and scanning transmission electron microscopy (STEM) with high-angle annular dark field (HAADF) imaging, combined EDS mapping and electron energy-loss spectroscopy (EELS), and transmission electron microscopy (TEM)/SAED. STEM/TEM is an inherently statistically poor tool for determining the relative amounts of particle types. However, the technique is much better at clearly identifying phases and compositions. A full report of the particle imaging and analysis can be found in Appendix E. Four samples were provided (AW-105 Solids 1, AW-105 Solids 2, Solution-1, Solution-3) and are presented in Table 4.10.

Table 4.10. Microscopy sample IDs.

Sample ID	Alternate ID	Content Description
AW-105 Solids-1	AW-105-19262	Core sample solids from tank AW-105, segment lower half centrifuged solids portion from core S06T000152 (Ritenour 2006)
AW-105 Solids-2	AW-105-20326	Core sample solids from tank AW-105, segment upper half settled solids portion from core S06T000152 (Ritenour 2006)
Filtered Solution-1	TI-177-S1	First backpulse solution of AW-105 feed.
Filtered Solution-3	TI-177-S3	Backpulse solution post 0.1 M NaOH filter cleaning

Materials representing AW-105 were sub-sampled for microscopy. Microscopy analysis types used on the four samples provided (two AW-105 core solids samples, Filtered Solution-1, and Filtered Solution-3) are detailed in Table 4.11. The core samples (AW-105 Solids-1, -2) contained dried solids that were only examined with SEM. Filtered Solution-1 and Filtered Solution-3 contained suspended particles in solution. These samples were also analyzed with SEM and then further sub-sampled for STEM analysis. The AW-105 Solids -1, -2 samples were deposited onto an SEM carbon stubs and analyzed. The Filtered Solution-1 and Filtered Solution-3 samples were pipetted onto carbon stubs. This process did result in the precipitation of salts; however, some useful information could still be obtained. The solutions were also prepared for STEM using the holey-carbon TEM grid as a filter that minimized evaporite formation. Only one sample could be analyzed with STEM (Filter Solution-1) due to mechanical problems with the JEOL GrandARM STEM.

Table 4.11. Sample analysis summary.

Samples	Techniques Applied	
	SEM	TEM
AW-105 Solids -1, -2	SEM, EDS mapping, particle analysis	Not attempted
Filtered Solution-1	SEM, EDS mapping	STEM/TEM/diffraction (SAED)/EDS mapping
Filtered Solution-3	SEM, EDS mapping	Instrument issues

All samples were analyzed during this investigation with the available tools. The AW-105 Solids segments were only examined on the SEM owing to the high activity and the size of the individual particles. The two filter samples consisted of particles suspended in solution. These were prepared by drop-casting onto an SEM stub and by drop-casting onto TEM grids. Although samples of Filtered Solution-3 were prepared for TEM, instrument issues prevented this analysis being completed. In general, STEM analysis can't provide useful data for particles more than 20 to 40 μm in diameter and several micrometers thick. However, SEM can easily accommodate these large particles. The objective of the drop-cast method was to limit the precipitation of salts. In some instances, this was not effective, and salts covered large areas of the sample during preparation

4.6.1 SEM Analysis of AW-105 Solids-1, -2

The SEM stubs prepared from the AW-105 Solids-1, -2 samples were dominated by zirconium phases and NaF. The NaF particles were tenaciously attached to the larger Zr-particles. There were also a few uranium particles in these specimens. Figure 4.6 presents a series of images at increasing magnification

showing highly heterogeneous particle agglomerates. Under back-scattered electron (BSE) imaging, the high Z particles show up clearly, and these were identified mainly as Zr-bearing (see Figure 4.7), iron-bearing (see Figure 4.8) and U-bearing particles (see Figure 4.9). However, one of the most common phases in AW-105, NaF (villiaumite), could not be distinguished with BSE contrast and was only observed in the elemental maps (see Figure 4.10). This meant that automated particle analysis using BSE contrast could not pick up this specific phase. The Zr-phase was a zirconium hydroxide.

The particles from the AW-105 that were mainly Zr-bearing were large, well over 100 μm in diameter, and might not be expected to be present in a supernatant.

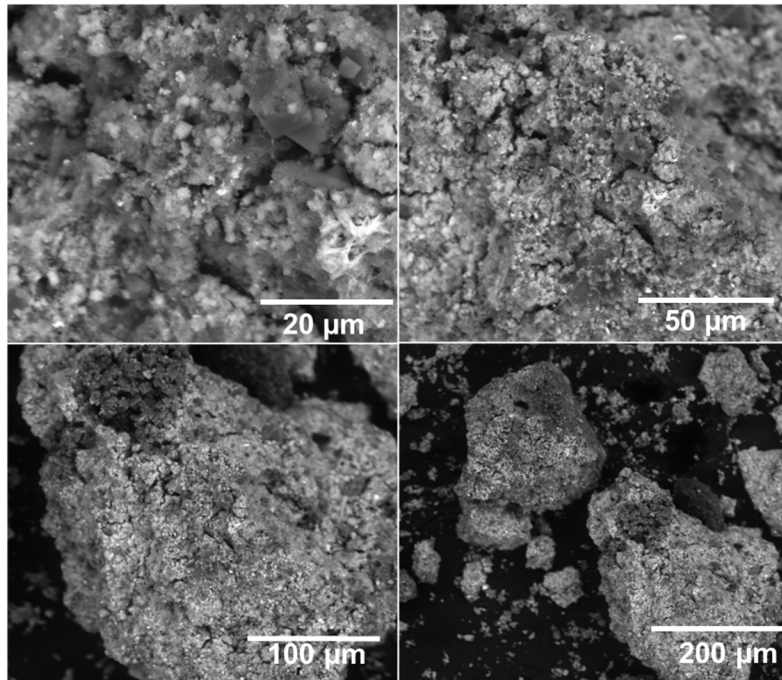


Figure 4.6. SEM images of AW-105 Solids-1 sample.

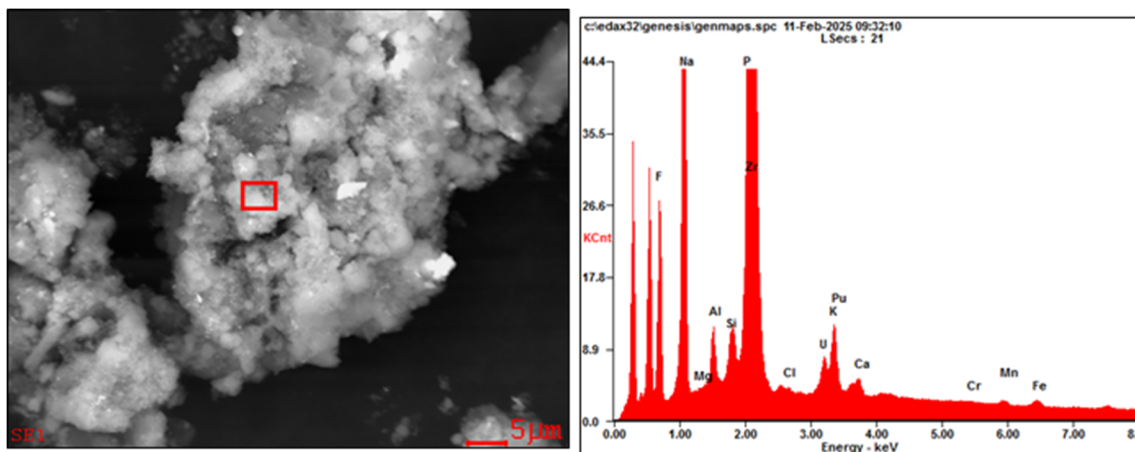


Figure 4.7. SEM image and EDS of Zr-hydroxide phase with a composition similar to that observed by Reynolds and co-workers (2014)

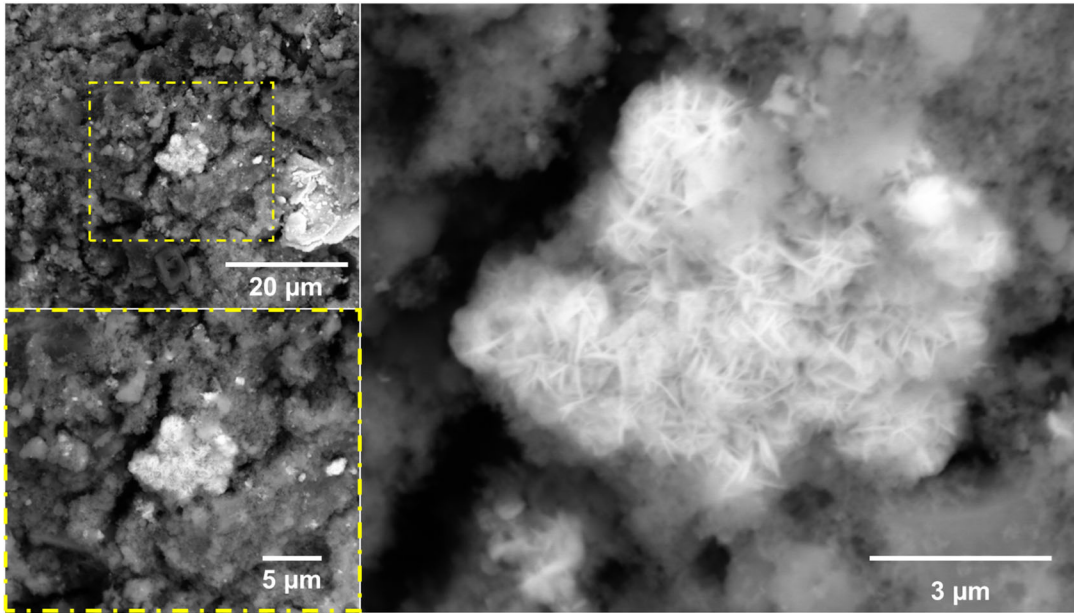


Figure 4.8. SEM images of AW-105 Solids-1 sample showing hematite particle agglomerate with a characteristic “rose-pellet” morphology.

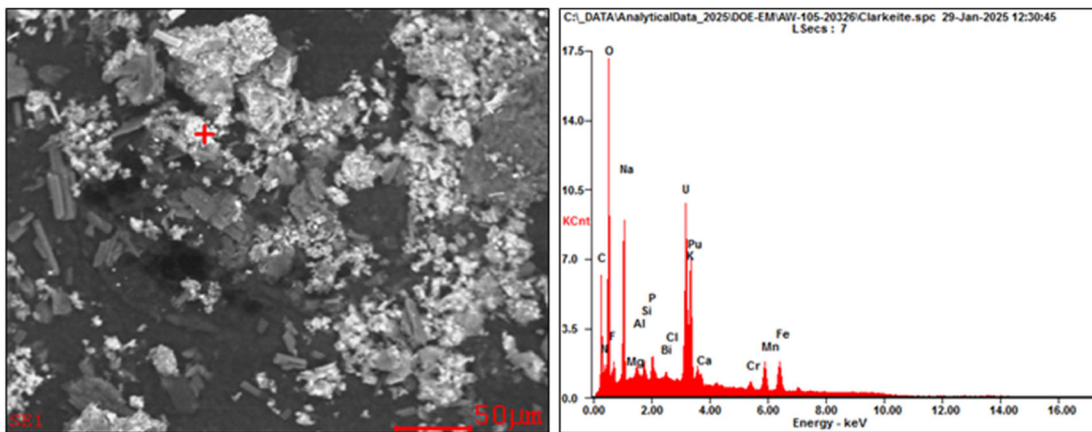


Figure 4.9. SEM images of various particles and an identified uranium-bearing phase consistent with clarkeite in the AW-105 Solids-2 sample.

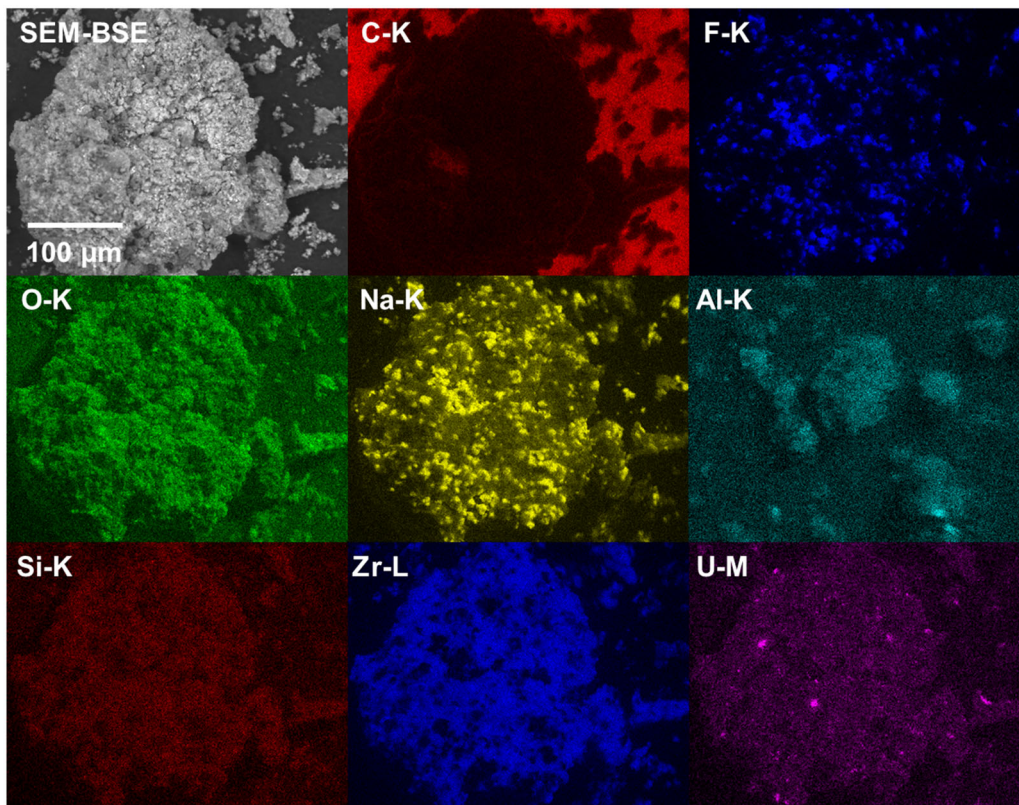


Figure 4.10. SEM image and EDS maps of particle agglomerates found in the AW-105 Solids-1 sample showing NaF particles and zirconium phases.

4.6.2 Filtered Solution-1

Several types of particles were observed with the SEM from Filtered Solution-1, including steel-like particles, uranium-bearing phases, and Mn-Fe phases. These particles were small, only a few micrometers in diameter. Figure 4.11 shows three different high Z particles that were identified in the SEM analysis of Filtered Solution-1. These included a Mn-Fe phase, a Ce-bearing phase, and particles consistent with a steel composition. In Figure 4.12, an elemental map shows the occurrence of the Mn-Fe phase. These phases were identified in the AW-105 sludge and can give an indication of the types of suspended phases that may be present elsewhere including the supernatant. Smaller Ca-bearing particles were also found.

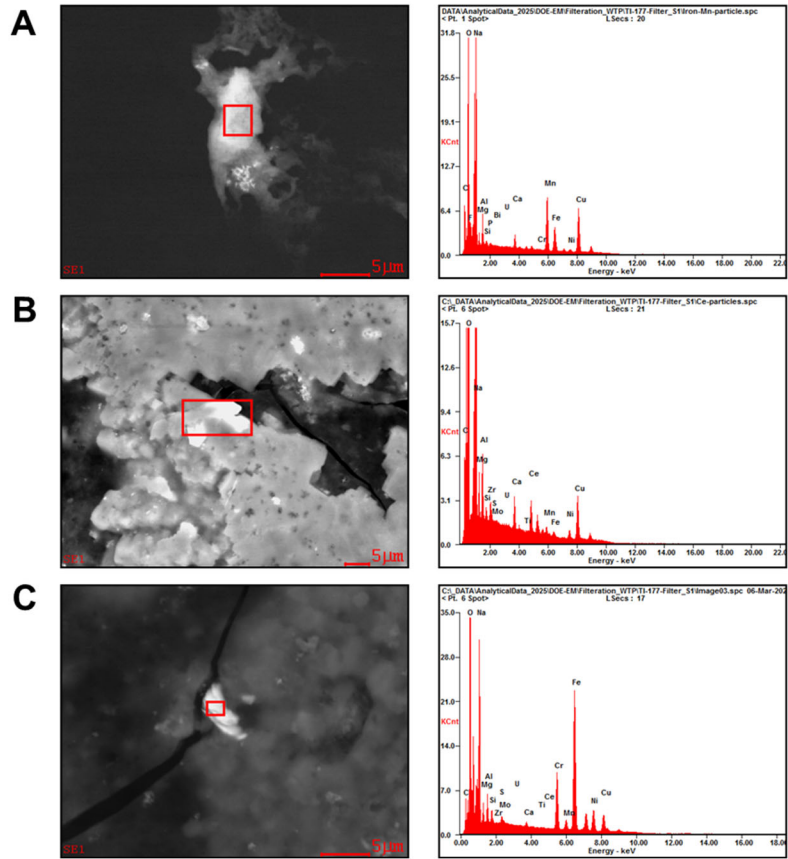


Figure 4.11. SEM images and EDS from particles observed in Filtered Solution-1. (A) Mn-Fe-phase, (B) cerium-bearing particle, and (C) steel particles.

In Figure 4.11, there is also a lot of salt material in the regions of interest. The highlighted particle (brighter contrast in the figures) is embedded in the darker contrast salt material. During the sample preparation, it was not possible to eliminate the salts from the sample.

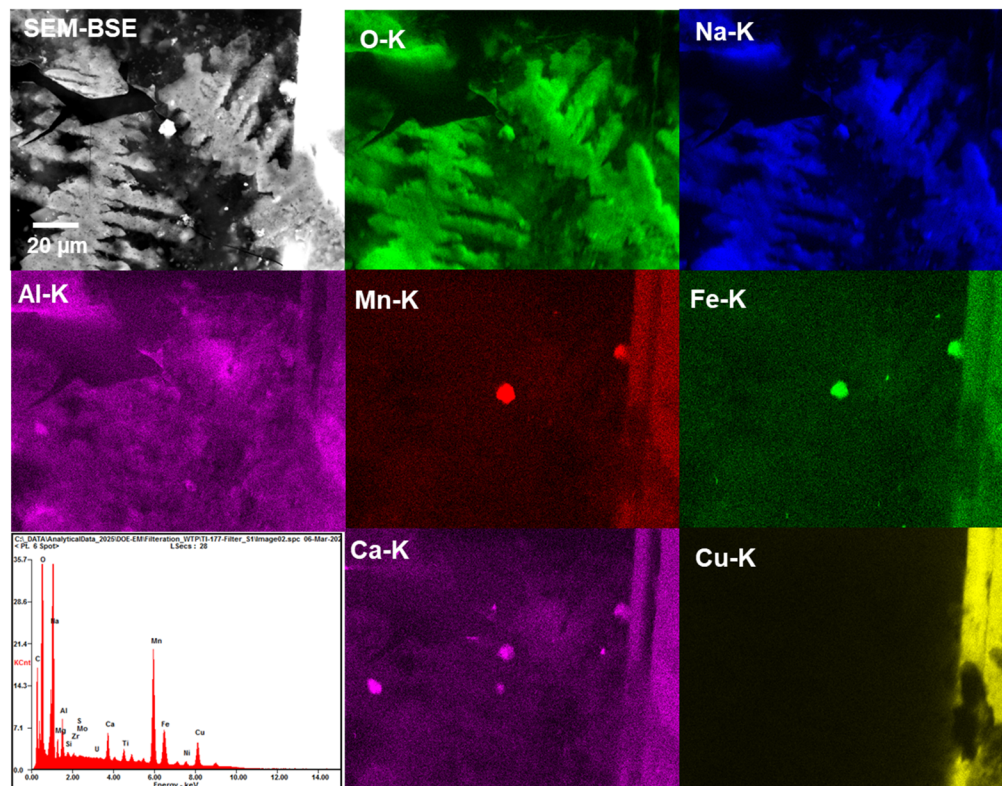


Figure 4.12. SEM and EDS analysis of a Mn-Fe and calcium particles associated with evaporated salt (that was not completely removed during sample preparation) from Filtered Solution-1.

Figure 4.13 shows a uranium-bearing phase. These particles were too small for more detailed analysis in the SEM and were partially buried in the evaporite material. The elemental map in Figure 4.14 shows a Zr-bearing particle from Filtered Solution-1. Automated particle Analysis (APA) was applied to the samples from Filtered Solution 1. Sodium dominated the specimen owing to evaporate formation; however, the higher Z particles were visible and could be identified with BSE contrast. The phase designations were made based on a best determination of the possible phase based on the EDS reported composition described in Figure 4.15. The plot shows a larger number of Zr-bearing particles in Filtered Solution-1. The total number of particles analyzed with the APA system from Filtered Solution-1 was 1,775.

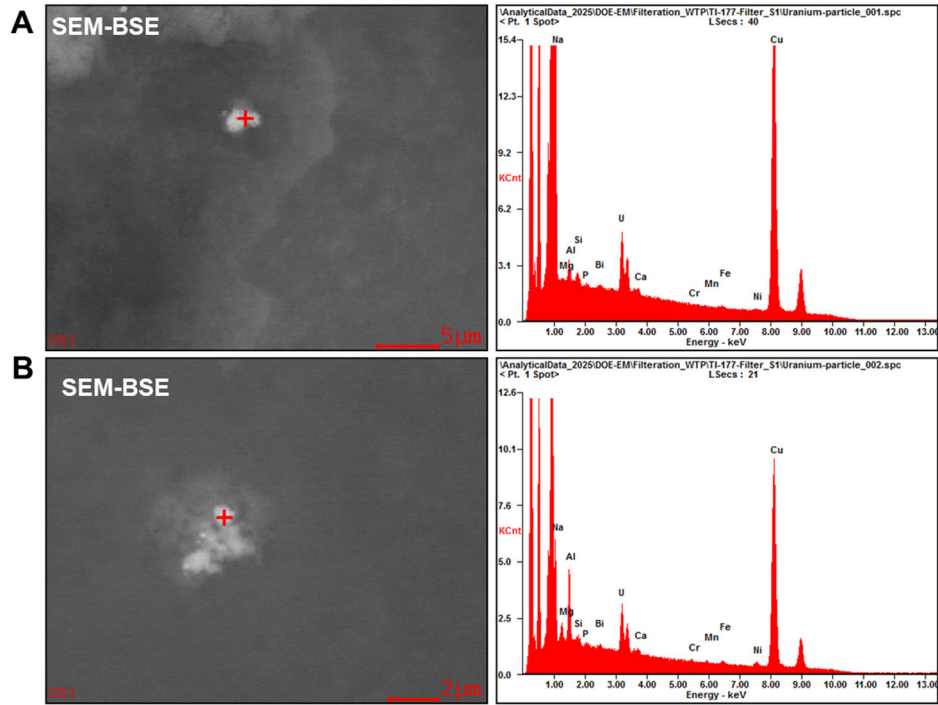


Figure 4.13. SEM images and EDS of uranium-bearing particles found in Filtered Solution-1.

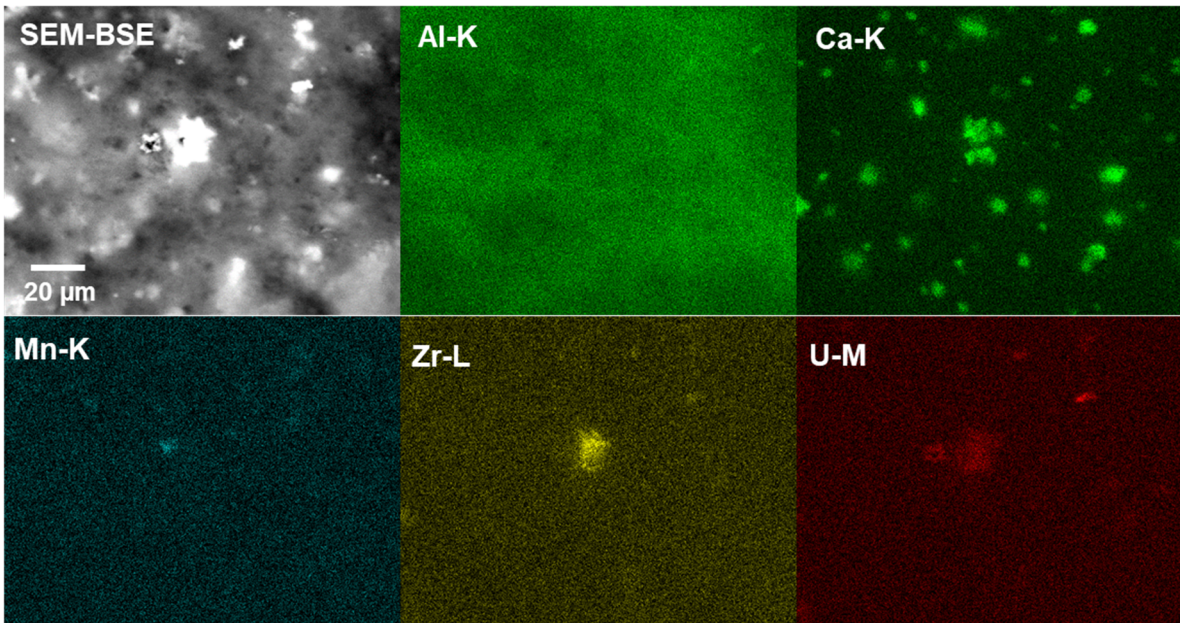


Figure 4.14. Elemental map showing a Zr-bearing particle from Filtered Solution-1 together with Ca-bearing particles.

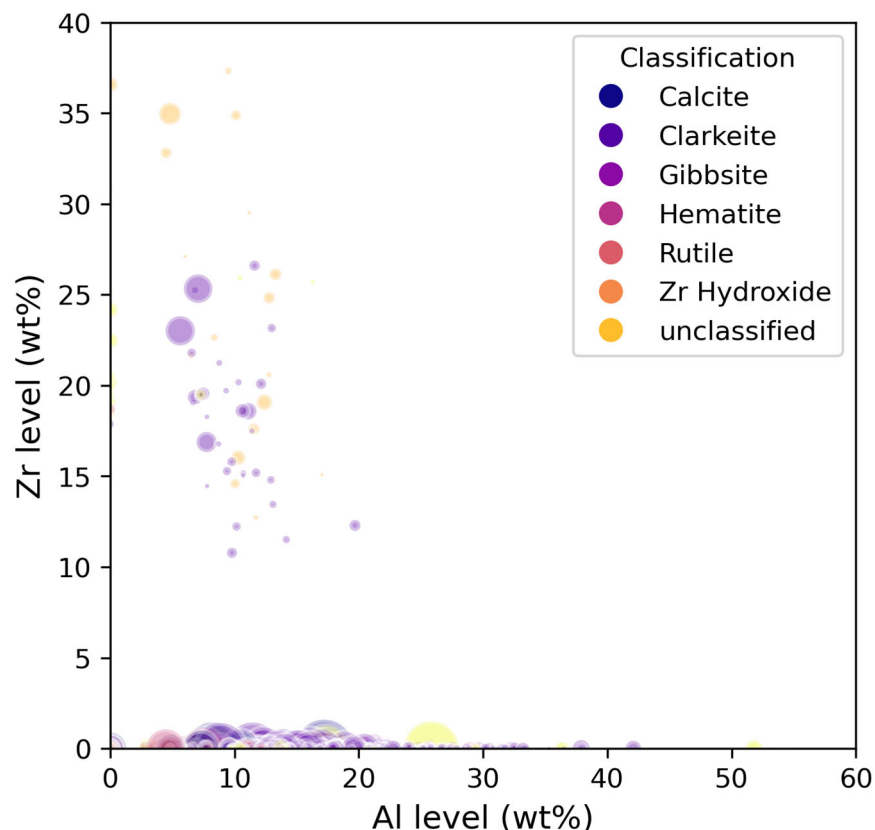


Figure 4.15. Particles containing Zr from the Filtered Solution-1. Unclassified refers to particles that were not uniquely identified during the analysis. Over 1200 particles were analyzed.

4.6.3 Filtered Solution-3

Macro observations noted Filtered Solution-3 had fewer particles when compared to the Filtered Solution-1 sample. These solids were examined using SEM. Again, this sample had a significant amount of evaporite solids that made imaging and analysis difficult. Little morphological information could be obtained from the SEM images of these particles as they were small (see Figure 4.16). The element maps in Figure 4.17 show the occurrence of Mn-bearing phases, Ca-bearing particles, and steel-like compositions. The elemental map for Al indicates there is a lot of this element in the sample, but it is more likely that this was dissolved Al rather than dissolved solids. Figure 4.18 shows an image and the spectrum from a uranium-bearing particle. The U-particle was about 3 to 4 μm in diameter.

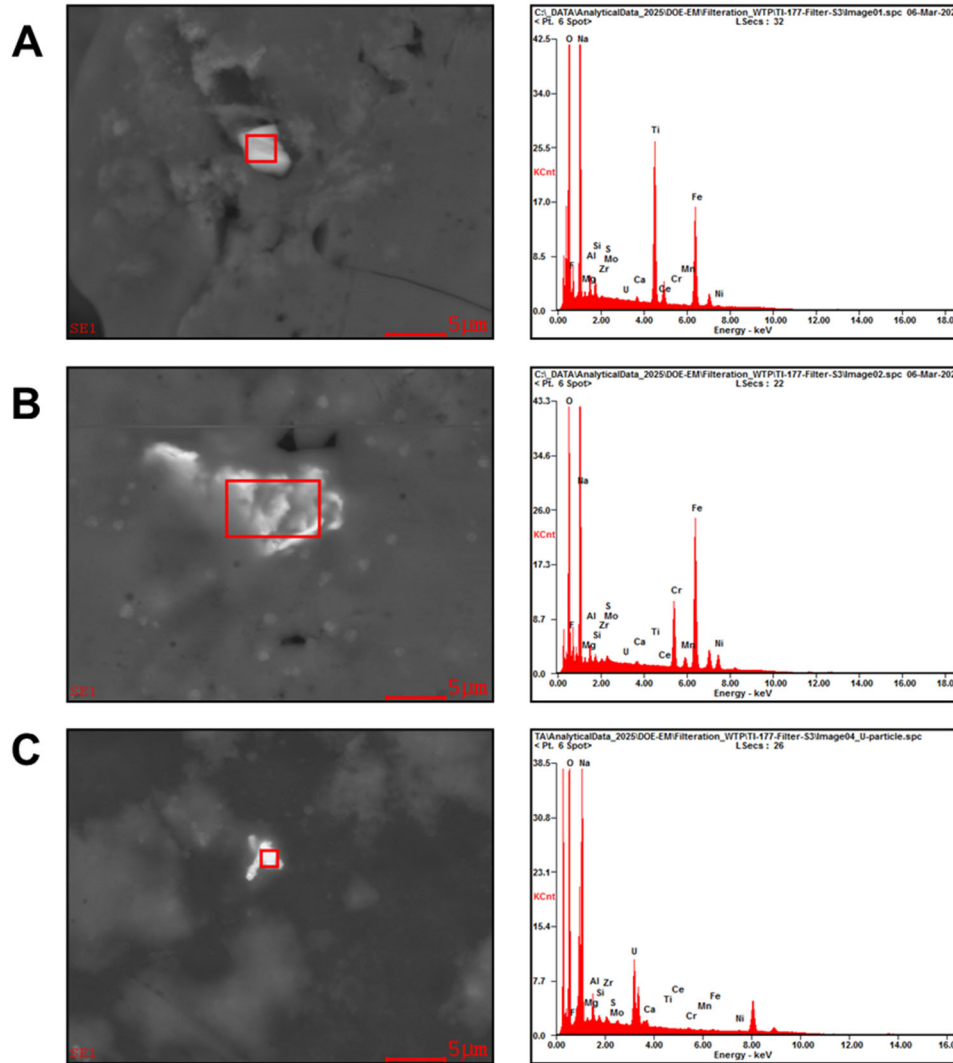


Figure 4.16. SEM images of particles observed in Filtered Solution-3 with EDS analyses. (A) Ti-bearing particle, (B) Fe-Cr-steel particle, and (C) a uranium-bearing particle.

The particles were not clearly visible, and the morphology could not be determined because these high Z particles were embedded in the evaporate material. Automated particle Analysis (APA) was applied to the samples from Filtered Solution-3. Sodium dominated the specimen owing to evaporate formation; however, the higher Z particles were visible and could be identified with BSE contrast. The phase designations were made based on a best determination of the possible phase based on the EDS reported composition described in Figure 4.19. The total number of particles analyzed with the APA system from Filtered Solution-3 was 3,318.

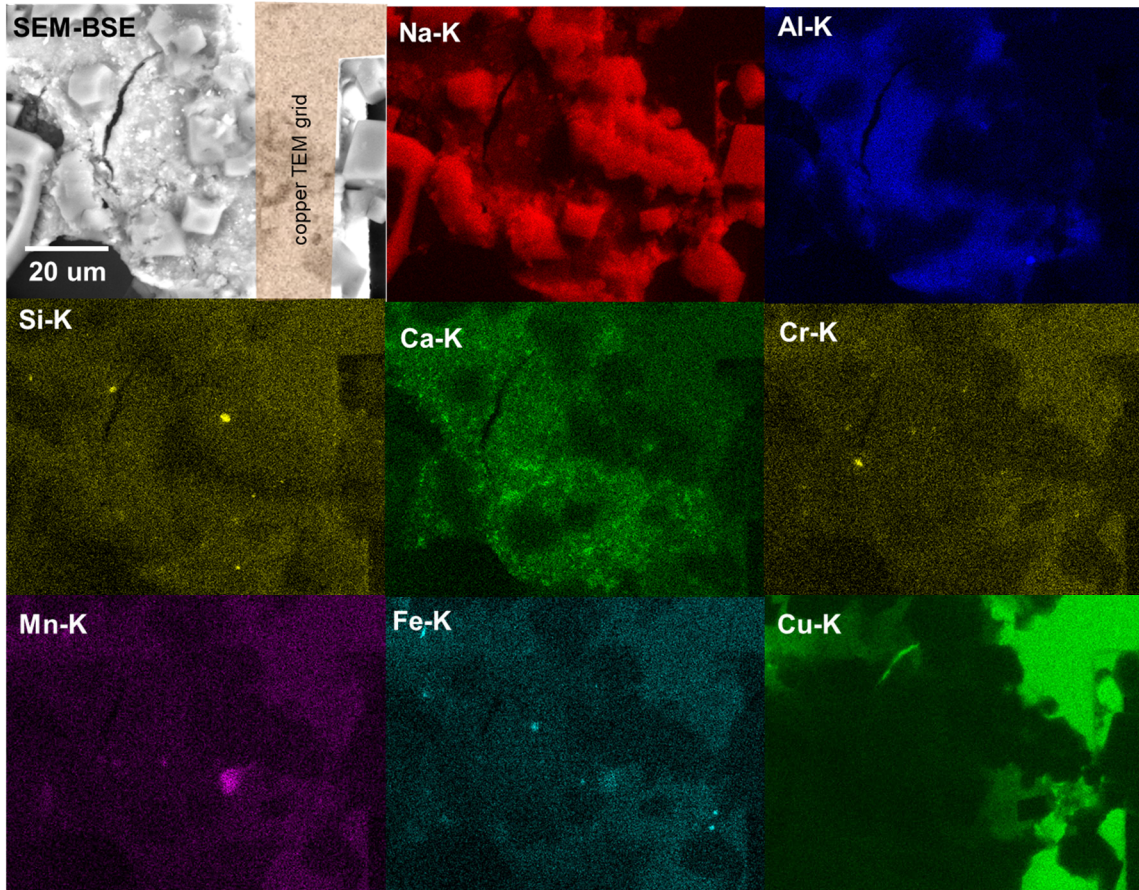


Figure 4.17. SEM image with highlighted Cu-grid and EDS elemental maps of Filtered Solution-3 showing the occurrence of a few Si, Cr-Fe, and Mn particles but many Ca-bearing phases.

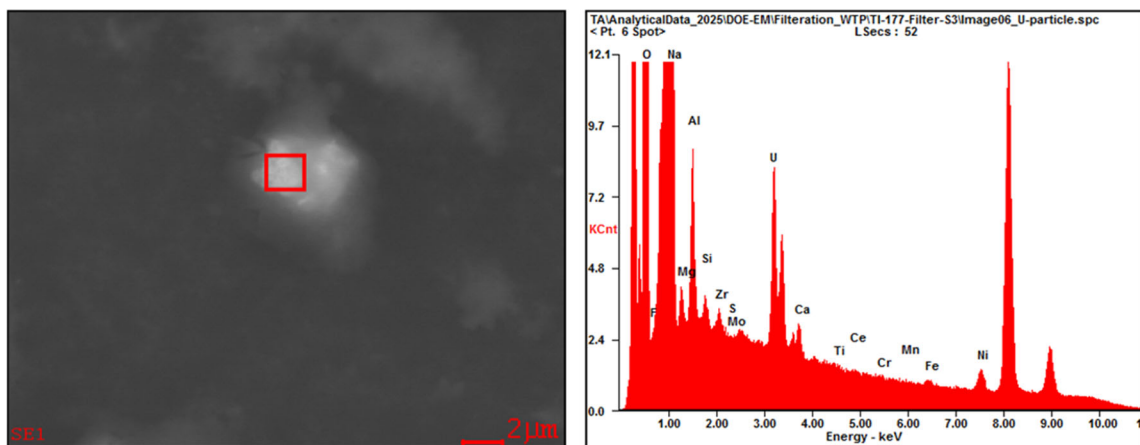


Figure 4.18. SEM image and EDS spectrum of a uranium-bearing particle in Filtered Solution-3.

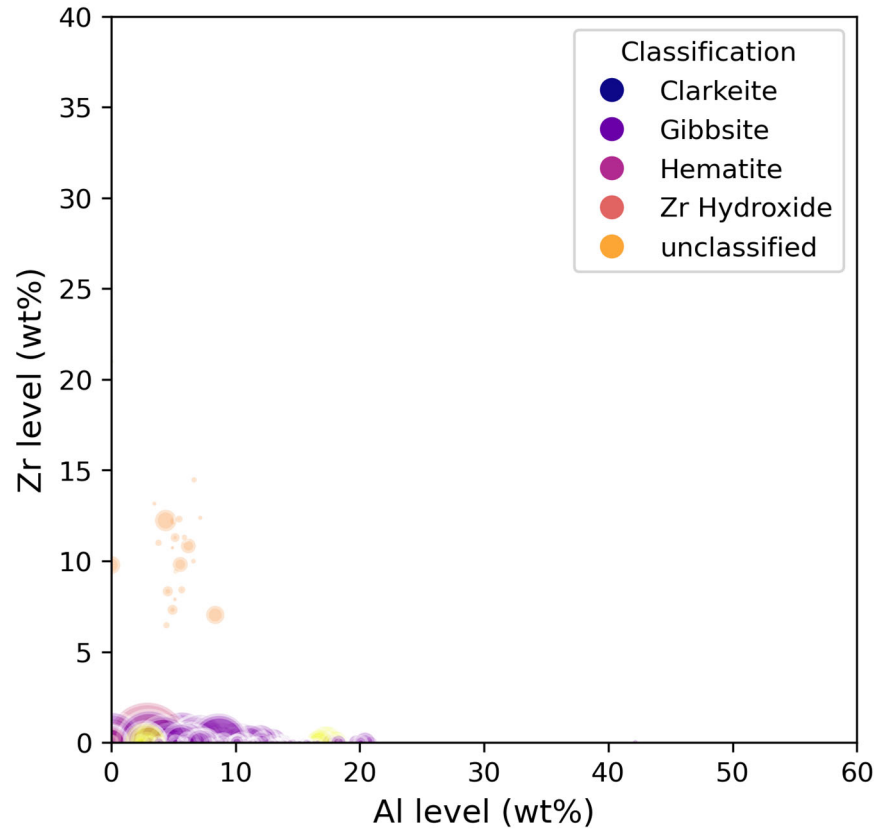


Figure 4.19. Particles containing Zr from the Filtered Solution-3. Over 3,000 particles were analyzed. The bright yellow in the figure represents the 'unclassified' particles.

5.0 Conclusions

Based on the results of the filtration experiments on supernatant waste from tank 241-AW-105 at 16 °C, the following observations and conclusions were made:

- Throughout filtration, the differential pressure required to effect filtration at 0.065 gpm/ft² increased slowly over the majority of the filtration campaign, but then increased significantly once feed bottoms were filtered, exceeding the TSCR action limit of 2 psid at 8.02 m³/m². This indicates that the Media Grade 5 filter could foul quickly when processing AW-105 supernatant that has not had sufficient time to settle. An intermediate blocking model coincides significantly with the AW-105 filtration resistance data.
- The prototypic filter cleaning process was sufficient in restoring filter performance after filtering AW-105 supernatant.
- The filtered permeate samples all had total alpha content less than the 0.1 μCi/g threshold defining TRU waste per DOE M 435.1-1, *Radioactive Waste Management Manual*.
- Solids concentrated from the backpulse solutions were composed of steel-like particles, uranium-bearing phases, Mn-Fe phases, a Ce-bearing phase, Zr hydroxide phases, and some smaller Ca-bearing particles. The Ca-bearing and U-bearing phases were identified as calcite and clarkeite, respectively with STEM analysis.

6.0 References

Allred, J. R., C. Alvarez, E. C. Buck, C. A. Burns, R. C. Daniel, J. E. Turner, A. M. Westesen, and R. A. Peterson. 2024. *Filtration of Hanford Tank 241-AN-107 Supernatant at 16 °C*. PNNL-35956, Rev. 0 (DFTP-RPT-041, Rev. 0). Pacific Northwest National Laboratory, Richland, Washington.

Allred, J. R., C. Alvarez, E. C. Buck, C. A. Burns, R. C. Daniel, J. G. H. Geeting, A. M. Westesen, and R. A. Peterson. 2023a. *Fiscal Year 2023 Filtration of Hanford Tank 241-SY-101 Supernatant at 16 °C*. PNNL-34509, Rev. 0 (RPT-DFTP-039, Rev. 0). Pacific Northwest National Laboratory, Richland, Washington.

Allred, J. R., C. Alvarez, E. C. Buck, C. A. Burns, R. C. Daniel, J. G. H. Geeting, A. M. Westesen, and R. A. Peterson. 2023b. *Fiscal Year 2023 Filtration of Hanford Tank 241-AP-105 Supernatant at 16 °C*. PNNL-34265, Rev. 0 (RPT-DFTP-036, Rev. 0). Pacific Northwest National Laboratory, Richland, Washington.

Allred, J. R., E. C. Buck, C. C. Burns, R. C. Daniel, J. G. H. Geeting, Z. B. Webb, A. M. Westesen, and R. A. Peterson. 2022. *Fiscal Year 2022 Filtration of Hanford Tank 241-AP-101 Supernatant at 16 °C*. PNNL-32851, Rev. 0 (RPT-DFTP-032, Rev. 0). Pacific Northwest National Laboratory, Richland, Washington.

Allred, J. R., J. G. H. Geeting, A. M. Westesen, E. C. Buck, and R. A. Peterson. 2021. *Fiscal Year 2021 Filtration of Hanford Tank 241-AP-107 Supernatant Samples Obtained at Prototypic Tank Level and Filtered at 16 °C*. PNNL-31557, Rev. 0 (RPT-DFTP-028, Rev. 0). Pacific Northwest National Laboratory, Richland, Washington.

Allred, J. R., J. G. H. Geeting, A. M. Westesen, E. C. Buck, and R. A. Peterson. 2020. *Fiscal Year 2020 Filtration of Hanford Tank Waste 241-AP-105*. PNNL-30485, Rev. 0 (RPT-DFTP-021, Rev. 0). Pacific Northwest National Laboratory, Richland, Washington.

Anderson, M. A. 2024. Waste Compatibility Assessment for the Transfer of Waste from Tank 241-AP-101 to Tank 241-AW-105. RPP-RPT-64795, Rev. 2A. Washington River Protection Solutions, Richland, Washington.

ASME. 2012. *Quality Assurance Requirements for Nuclear Facility Applications*. NQA-1-2012. The American Society of Mechanical Engineers, New York, New York.

Garrard, WN. 2024a. *Tank 241-AW 105 Large Volume Sample Collection to Support Platform Testing, Phase 1, FY24*. RPP-PLAN-66379, Rev. 0, Washington River Protection Solutions, Richland, Washington.

Garrard, WN. 2024b. *Tank 241-AW 105 Large Volume Sample Collection to Support Platform Testing, Phase 2, FY24*. RPP-PLAN-66402, Rev. 0, Washington River Protection Solutions, Richland, Washington.

Gerber, M. S. 1992. *Legend and Legacy: Fifty Years of Defense Production at the Hanford Site*. WHC-MR-0293, Rev. 2. Westinghouse Hanford Company, Richland, Washington. doi:10.2172/10144167

Hermia, J. 1982. "Constant Pressure Blocking Filtration Laws – Application to Power-Law Non-Newtonian Fluids." *Transactions of the Institution of Chemical Engineers* 60(3):183-187.

Ritenour G. 2006. Final Report For Tank 241-AW-105 Core 322 Samples For The Corrosion Mitigation And Criticality Programs. RPP-RPT-29745 Rev.0A. CH2M Hill, Richland, Washington.

Reynolds, J. G., H. J. Huber, G. A. Cooke, and J. A. Pestovich. 2014. "Solid-Phase Zirconium and Fluoride Species in Alkaline Zircaloy Cladding Waste at Hanford." *Journal of Hazardous Materials* 278: 203-210. <https://doi.org/10.1016/j.jhazmat.2014.05.097>.

Appendix A – BDEF Piping and Instrumentation Diagram

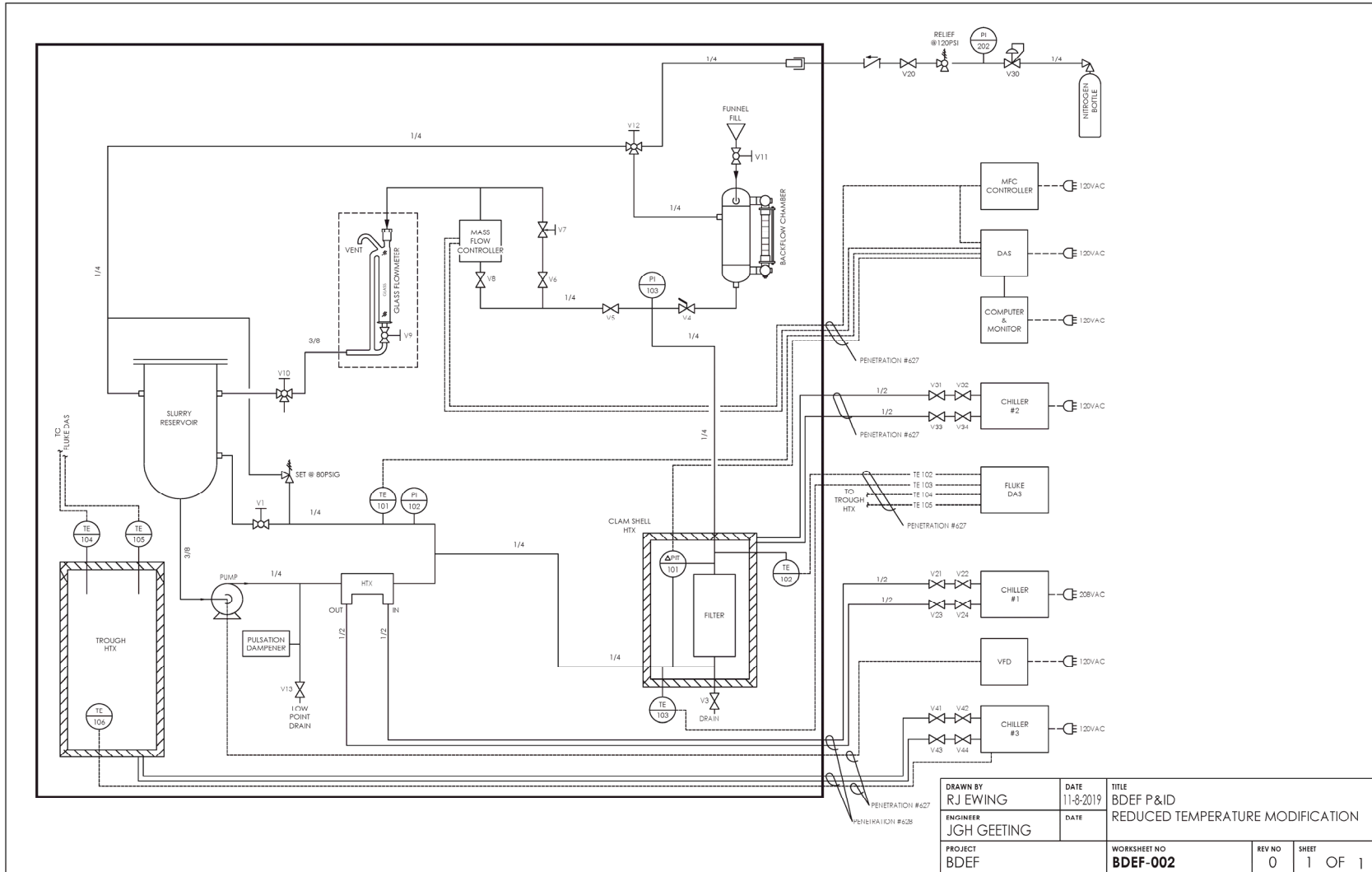


Figure A.1. BDEF piping and instrumentation diagram.

Appendix B – Feed Bottle Composite and Dilution

Composite Bottle ID	Receipt Sample Jar ID	Sample Location (depth below liquid surface, inches)	Waste Mass Addition to Composite Bottle (g)	Water Addition to Composite Bottle (g)	
BDEF-AW5-1	5AW-24	-01	39	1229.3	148.6
	5AW-24	-10	116		
	5AW-24	-19	194		
	5AW-24	-28	271		
BDEF-AW5-2	5AW-24	-02	39	1264.9	152.6
	5AW-24	-11	116		
	5AW-24	-20	194		
	5AW-24	-29	271		
BDEF-AW5-3	5AW-24	-03	39	1258.9	151.7
	5AW-24	-12	116		
	5AW-24	-21	194		
	5AW-24	-30	271		
BDEF-AW5-4	5AW-24	-04	39	1262.5	154.0
	5AW-24	-13	116		
	5AW-24	-22	194		
	5AW-24	-31	271		
BDEF-AW5-5	5AW-24	-05	39	1269.9	158.0
	5AW-24	-14	116		
	5AW-24	-23	194		
	5AW-24	-32	271		
BDEF-AW5-6	5AW-24	-06	39	1242.8	149.3
	5AW-24	-15	116		
	5AW-24	-24	194		
	5AW-24	-33	271		
BDEF-AW5-7	5AW-24	-07	39	1258.6	151.9
	5AW-24	-16	116		
	5AW-24	-25	194		
	5AW-24	-34	271		
BDEF-AW5-8	5AW-24	-08	39	1222.8	148.0
	5AW-24	-17	116		
	5AW-24	-26	194		
	5AW-24	-35	271		
BDEF-AW5-9	5AW-24	-09	39	921.5	110.7
	5AW-24	-27	194		
	5AW-24	-36	271		

Appendix C – Total Alpha Analysis for Filtration Permeate Samples

Pacific Northwest National Laboratory
 Richland, WA
 Radiochemical Sciences and Engineering Group

Filename: ASR 2198 Allred Total Alpha
 2/12/2025

Client: J. Allred Project: 84297
 ASR: 2198 Charge code: NU8946

Prepared by: Lawrence R Greenwood
Digitally signed by Lawrence R Greenwood
 Date: 2025.02.12 14:42:22 -08'00'

Concur: Truc Trang-Le
Digitally signed by Truc Trang-Le
 Date: 2025.02.12 14:32:05 -08'00'

Procedure: Activity #6556- Preparation of Samples for Gross Alpha and Beta
 M & TE: Ludlum Alpha Detectors
 Count date: 11-Feb-25

RPL ID:	Sample ID:	Total Alpha Activity, uCi/g ± 1s	
25-0431	TI-177-P1	2.04E-04	± 4%
25-0431 dup		2.08E-04	± 4%
25-0432	TI-177-P2	4.06E-05	± 16%
25-0432 dup		4.51E-05	± 13%
25-0433	TI-177-P3	7.29E-05	± 8%
25-0433 dup		7.77E-05	± 10%
25-0431 PB		-7.80E-08	± 29%
25-0431 BS		80%	
25-0431 MS		69%	
25-0432 MS		67%	
25-0433 MS		51%	

The first total alpha measurements showed high alpha absorption due to the mass of sample deposited on the counting plates resulting in MS yields of about 47%. The samples were reprepared by diluting the samples a factor of 13 resulting in only about 1.7 mg on each counting plate. The MS yields were much higher as shown in the table.

Appendix D – ICP-OES Analysis for Diluted and Compositd 241-AW-105 Supernatant

Battelle PNNL/RPG/Inorganic Analysis ... ICPOES Data Report

Run Date >	1/27/2025	1/27/2025	1/27/2025	1/27/2025	1/27/2025	1/27/2025	1/27/2025	1/27/2025	1/27/2025	1/27/2025	1/27/2025	1/27/2025	
Process Factor >	1.0	1.0	1.0	131.6	121.1	1329.1	1216.3	135.1	139.9	1346.3	1405.8		
	405 Diluent	25-0434 PB @1x	25-0434 PB @1x HF	25-0434 @10x	25-0434 Dup @10x	25-0434 @50x	25-0434 Dup @50x	25-0434 @10x HF	25-0434 Dup @10x HF	25-0434 @50x HF	25-0434 Dup @50x HF		
Instr. Det. Limit (IDL)	Est. Quant. Limit (EQL)	Client ID >				BDEF-AW5-D	BDEF-AW5-D	BDEF-AW5-D	BDEF-AW5-D	BDEF-AW5-D	BDEF-AW5-D	BDEF-AW5-D	
(µg/mL)	(µg/mL)	(Analyte)	(µg/g)	(µg/g)	(µg/g)	(µg/g)	(µg/g)	(µg/g)	(µg/g)	(µg/g)	(µg/g)	(µg/g)	
0.0091	0.091	Al	--	[0.026]	0.154	6.790	6.680	6.850	7.020	6.800	6.680	6.760	6.870
0.1768	1.768	As	--	--	--	--	--	--	--	--	--	--	--
0.0002	0.002	Ba	[0.0003]	[0.0002]	[0.0003]	[0.10]	[0.11]	[0.26]	--	[0.085]	[0.10]	[0.22]	[0.23]
0.0075	0.075	Ca	[0.043]	[0.025]	[0.021]	[1.7]	[5.8]	[72]	[65]	[2.4]	[6.1]	158	122
0.0079	0.079	Cd	--	--	--	--	--	--	--	--	--	--	--
0.0046	0.046	Cr	--	--	--	256	250	264	273	246	246	255	262
0.0025	0.025	Fe	--	0.0330	0.0392	[3.2]	[2.5]	[4.9]	[3.7]	[2.6]	[2.5]	[3.7]	--
0.0352	0.352	K	--	[0.22]	--	18.800	18.600	16.900	17.400	18.400	17.900	16.500	17.200
0.0085	0.085	Na	[0.036]	0.133	[0.064]	103.000	99.700	107.000	109.000	98.200	98.600	102.000	106.000
0.0085	0.085	Ni	--	--	--	[4.8]	[5.5]	--	--	[5.2]	[4.4]	[13]	--
0.1778	1.778	P	--	--	--	356	332	[490]	[320]	335	322	[510]	[380]
0.0385	0.385	Pb	[0.056]	--	[0.065]	[11]	[9.8]	[63]	[67]	[7.8]	[9.8]	--	--
0.6450	6.450	S	--	--	--	1.040	1.010	[1.200]	--	971	971	--	--
0.0002	0.002	Sr	--	--	--	[0.028]	[0.036]	--	--	--	--	--	--
0.0007	0.007	Ti	--	--	[0.0026]	--	--	--	--	--	[0.11]	--	--
0.0675	0.675	U	--	--	--	--	--	--	--	--	--	--	--
0.0087	0.087	Zn	--	[0.035]	[0.027]	[5.9]	[4.7]	[56]	[57]	[5.6]	[5.4]	[54]	[54]
0.0018	0.018	Zr	--	--	--	[1.1]	[1.2]	--	--	[1.1]	[1.0]	--	--
Other Analytes													
0.0022	0.022	Ag	--	--	--	--	--	--	--	--	--	--	--
0.0193	0.193	B	--	--	--	[17]	[16]	[30]	[26]	[16]	[16]	--	--
0.0001	0.001	Be	--	--	--	1.47	1.43	1.58	1.50	1.41	1.41	1.45	1.55
0.0618	0.618	Bi	--	--	--	--	--	--	--	--	--	--	--
0.0163	0.163	Ce	--	--	--	--	--	--	--	--	--	--	--
0.0064	0.064	Co	--	--	--	--	--	--	--	--	--	--	--
0.0019	0.019	Cu	--	--	[0.0063]	4.96	4.81	[2.8]	[4.4]	4.48	4.84	--	[3.5]
0.0034	0.034	Dy	--	--	--	--	--	--	--	--	--	--	--
0.0006	0.006	Eu	--	--	--	--	--	--	--	--	--	--	[1.2]
0.0018	0.018	La	--	--	--	--	--	--	--	--	--	--	--
0.0015	0.015	Li	--	[0.0057]	--	[1.1]	[0.45]	[2.0]	--	[0.40]	[0.42]	[2.5]	--
0.0025	0.025	Mg	--	[0.0052]	[0.0055]	[0.75]	[0.88]	[5.2]	--	[0.44]	[0.76]	54.4	[6.0]
0.0007	0.007	Mn	--	--	--	[0.90]	0.984	--	[1.00]	[0.81]	[0.85]	[1.0]	[1.2]
0.0173	0.173	Mo	--	--	--	[13]	[13]	--	--	[13]	[15]	--	--
0.0126	0.126	Nd	--	--	--	--	--	--	--	--	--	--	--
0.0113	0.113	Pd	--	--	--	[2.5]	[1.7]	--	--	--	--	--	--
0.0389	0.389	Rh	--	--	--	--	--	--	--	--	--	--	--
0.0128	0.128	Ru	--	--	--	[5.1]	[5.0]	--	--	[3.5]	[4.1]	--	--
0.1139	1.139	Sb	--	--	--	--	--	--	--	--	[17]	--	--
0.4064	4.064	Se	--	--	--	--	--	--	--	--	--	--	--
0.0212	0.212	Si	[0.027]	0.652	8.07	[9.1]	[6.3]	[51]	[37]	53.9	59.3	[31]	[44]
0.1168	1.168	Sn	--	--	--	[71]	[51]	--	--	[64]	[41]	--	--
0.0320	0.320	Ta	--	--	--	--	--	--	--	--	--	--	--
0.0623	0.623	Te	--	--	--	--	--	--	--	--	--	--	--
0.0116	0.116	Th	--	--	--	--	--	--	--	--	--	--	--
0.1934	1.934	Tl	--	--	--	--	--	--	--	--	--	--	--
0.0029	0.029	V	--	--	--	--	--	--	--	--	--	--	--
0.0513	0.513	W	--	--	--	[25]	[25]	--	--	[21]	[24]	--	--
0.0006	0.006	Y	--	--	--	--	--	--	--	--	--	--	--

1) "--" indicates the value is < MDL. The method detection limit (MDL) = IDL times the "multiplier" near the top of each column. The estimated sample quantitation limit = EQL (in Column 2) times the "multiplier". Overall error for values ≥ EQL is estimated to be within ±15%.

2) Values in brackets [] are ≥ MDL but < EQL, with errors likely to exceed 15%.

na = not applicable; KOH flux and Ni crucible or Na₂O₂ flux and Zr crucible for fusion preparations, or Si for HF assisted digests.

Battelle PNNL/RPG/Inorganic Analysis ... ICPOES Data Report

QC Performance 1/27/2025

Criteria >	≤ 20%	80%-120%	75%-125%	75%-125%	80%-120%	80%-120%	≤ 10%
QC ID >	25-0434 @10x Dup	LCS/BS	25-0434 @10x MS	25-0434 @10x BS	25-0434 @10x HF + PSA	25-0434 @10x HF + PSB	25-0434 Dup @50x 10-fold Serial Dil
Analytes	RPD (%)	%Rec	%Rec	%Rec	%Rec	%Rec	%Diff
Al	6.8	100	97	93	98		4.6
As		99	101	101	96		
Ba		102	96	94	97		
Ca		98	92	90	96		
Cd		102	95	94	99		
Cr	5.9	101	102	92	97		8.6
Fe		103	93	95	97		
K	7.1	97	105	90	96		6.7
Na	5.4	103	nr	100	98		8.9
Ni		104	92	93	95		
P	1.4	104	101	98	98		
Pb		101	93	93	97		
S	5.9	98	99	93		89	
Sr		100	89	89	97		
Ti		103	97	98	98		
U		101	89	91		96	
Zn		101	93	97	102		
Zr		104	101	99	100		
Other Analytes							
Ag		100			95		
B		101	94	97	97		
Be	5.6	102	92	94	98		4.5
Bi		93			90		
Ce		101	92	93		96	
Co		104			97		
Cu	5.1	111	100	99	103		
Dy		100				95	
Eu		99				93	
La		100	91	91		95	
Li		106	103	97	101		
Mg		103	93	95	99		
Mn		103	91	93	97		
Mo		101	98	96	93		
Nd		99	91	92		94	
Pd		96				91	
Rh		99				95	
Ru		95				90	
Sb		100			92		
Se		102			86		
Si		103			98		
Sn		107			100		
Ta		107			98		
Te		101				92	
Th		100	91	91		93	
Tl		95			91		
V		101	92	92	96		
W		105	92	87	96		
Y		100			97		

Shaded results are outside the acceptance criteria.

nr = spike concentration less than 25% of sample concentration. Matrix effects can be assessed from the serial dilution.

na = not applicable, KOH flux and Ni crucible or Na₂O₂ flux and Zr crucible for fusion preparations, or Si for HF assisted digests.

Appendix E – Microscopy Analysis of Backpulsed Solids from AW-105

To identify the solids in the filtered solutions of the AW-105 samples, this study used scanning transmission electron microscopy (STEM) with high-angle annular dark field (HAADF) imaging, combined EDS mapping and electron energy-loss spectroscopy (EELS), as well as TEM/SAED. This technique is excellent for identifying phases and compositions. This appendix contains several STEM/TEM analyses.

E.1 Experimental Procedure

Materials representing AW-105 were sub-sampled for STEM/TEM. Two samples were provided: Filtered Solution-1, and Filtered Solution-3, as outlined in Table E.1 and previously detailed in Table 4.10. The two samples (Filtered Solution-1 and Filtered Solution-3) contained suspended particles in solution. These were also analyzed with SEM and then further sub-sampled for STEM analysis. The solution samples were pipetted onto carbon stubs. This process did result in the precipitation of salts; however, useful information could still be obtained. The solutions were also prepared for STEM using the holey-carbon TEM grid as a filter to minimize evaporite formation. Only one sample could be analyzed with STEM (Filtered Solution-1) due to mechanical problems with the JEOL GrandARM STEM microscope.

Table E.1. Sample analysis summary.

Samples	Techniques Applied	
	SEM	TEM
Filtered Solution-1	SEM, EDS mapping	STEM/TEM/Diffraction (SAED)/EDS mapping
Filtered Solution-3	SEM, EDS mapping	Instrument issues

STEM/TEM analysis used a JEOL (JEOL Inc., Japan) ARM300F (GrandARM) microscope. STEM images were collected using a HAADF detector and compositional analysis was obtained with EDS. TEM-SAED patterns were analyzed with DigitalMicrograph 3.0 software and using scripts developed by Mitchell (2008) and CrysTBox (Crystallographic Tool Box) software (Klinger 2017). Crystallographic files for the phases of interest were obtained from the American Mineralogist Crystallographic Database (Downs and Hall-Wallace 2003).

E.2 Microscopy Solids Analysis Results

All samples were analyzed during this investigation with the available tools. The AW-105 Solids-1, -2 samples were only examined on the SEM owing to the high activity and the size of the individual particles. The two filtered samples consisted of particles suspended in solution. These were prepared by drop-casting onto an SEM stub and by drop-casting onto TEM grids. Although samples of Filtered Solution-3 were prepared for TEM, instrument issues prevented this analysis from being completed. In general, STEM analysis can't provide useful data for a particle that is more than 20 to 40 μm in diameter and several micrometers thick. However, with SEM, these large particles can be easily accommodated. The object of the drop-cast method was to limit the precipitation of salts. In some instances, this was not effective, and salts covered large areas of the sample preparations.

E.2.1 AW-105 TEM Analysis

The two filtered solution samples were prepared for TEM/STEM. However, only the Filtered Solution-1 could be examined using GrandARM 300F tool. Instrument issues beyond control prevented the Filtered Solution-3 sample from being examined.

E.2.2 STEM Analysis of Filtered Solution-1

Figure E.1 shows STEM-HAADF images and STEM-EDS elemental maps of a collection of different particles found in the Filtered Solution-1 sample.

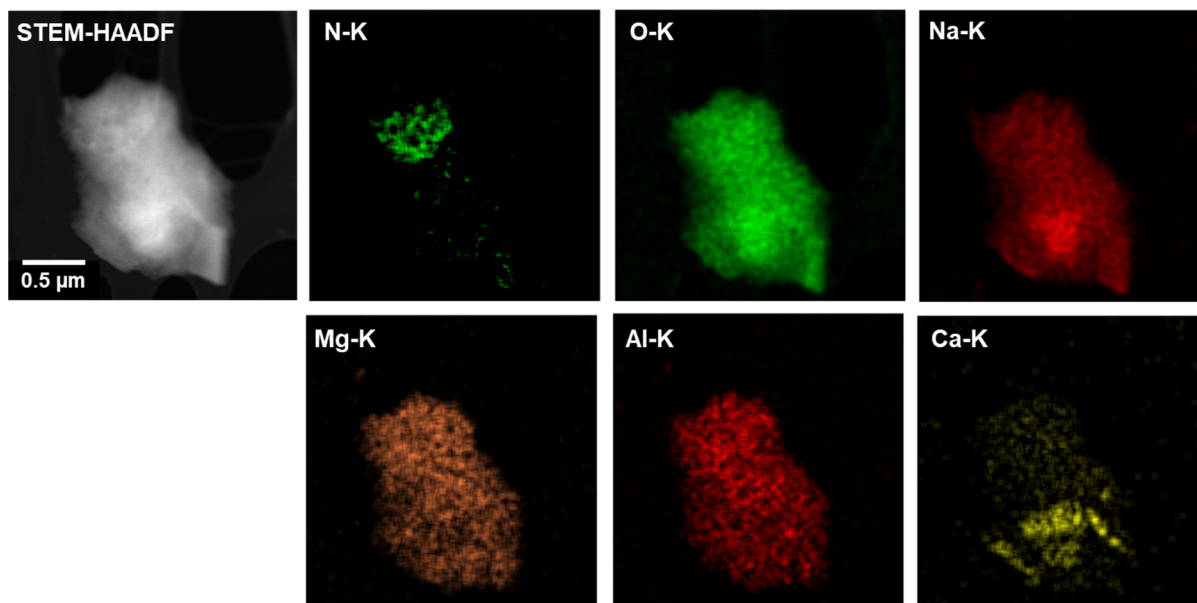


Figure E.1. HAADF image and STEM-EDS maps of sodium-rich particles, with an attached Ca-bearing phase in Filtered Solution-1.

Most of the particles proved to be amorphous or could have been damaged by the electron beam prior to analysis. Figure E.2 shows STEM-HAADF and STEM-EDS maps of a sodium-bearing phases, most likely evaporate material.

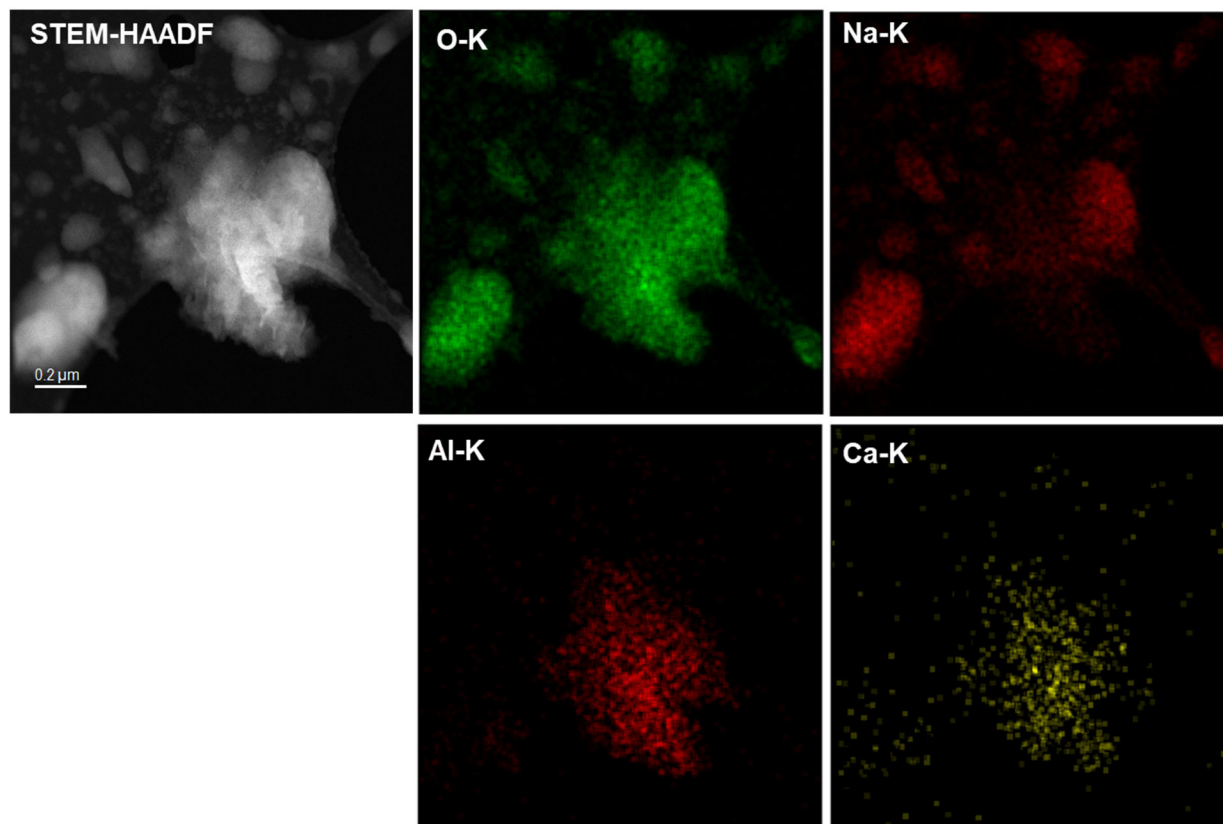


Figure E.2. HAADF image and STEM-EDS analysis of an evaporate particle that was commonly found in the TEM sample.

Images and diffraction patterns of these phases were also captured. However, the diffraction was weak (see Figure E.3) and could not be identified positively as a specific phase. An attempt was made to match the results to villiaumite (NaF), but no match could be made.

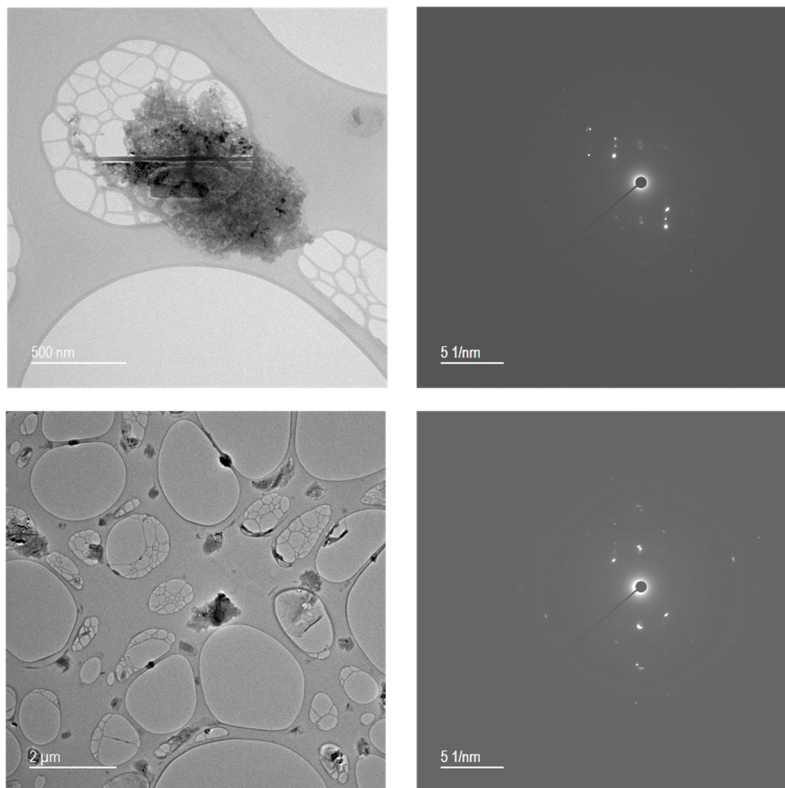


Figure E.3. TEM images and electron diffraction patterns of a particle agglomerate in Filtered Solution-1.

Figure E.4 shows a TEM image of the Filtered Solution-1 specimen, indicating the possible presence of a few undissolved solids. The mass of the material was most likely evaporite material.

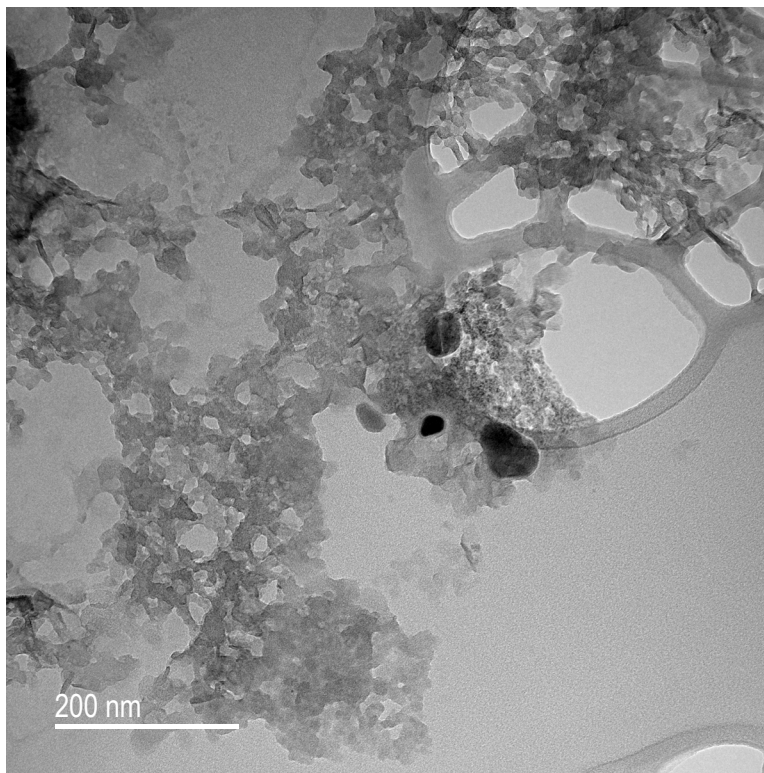


Figure E.4. TEM images of particles observed in the Filtered Solution-1 sample.

E.2.2.1 Calcium-Bearing Phase in Filtered Solution-1

Calcium-bearing particles were found throughout Filtered Solution-1 in the STEM analysis. These occurred as elongated particles. The elemental maps in Figure E.5 and Figure E.6 show the Ca distribution. Electron energy-loss spectroscopy was attempted on the Ca phase and the results are shown in Figure E.6. Quantification of light elements was accomplished with EELS, and these indicate a Ca/O ratio (24/72 at%), which would be consistent with calcite (CaCO_3). The carbon content was impacted by the C-support film. SAED of these particles is shown in Figure E.7, and the resulting pattern was matched with calcite. There was a reasonable agreement with this phase.

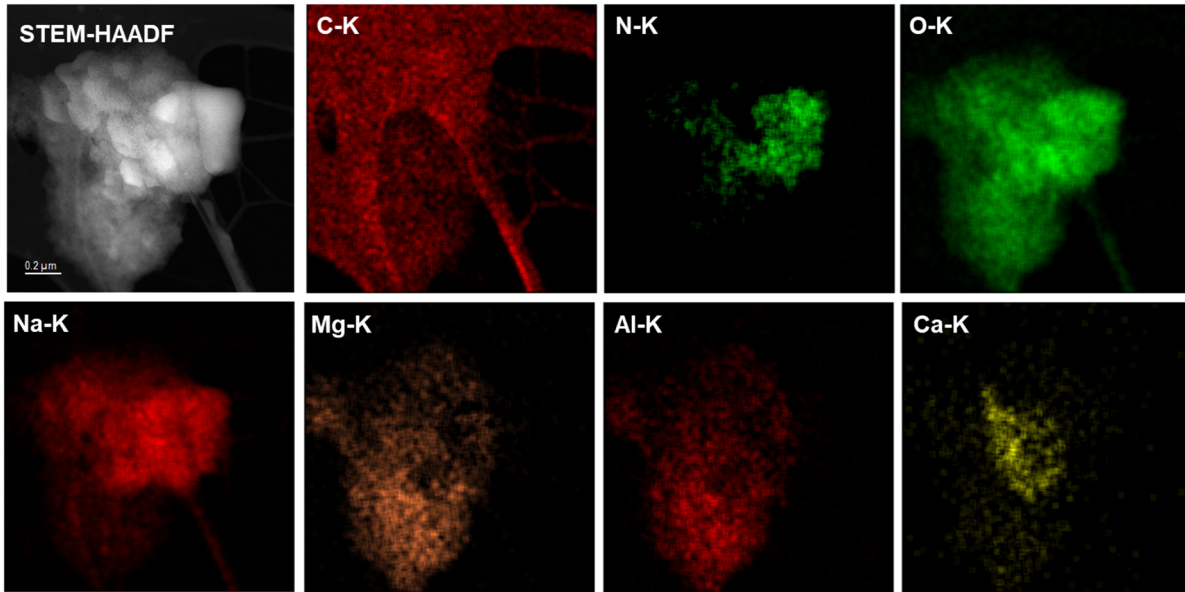


Figure E.5. STEM image and EDS elemental maps of a particle consisting of an Al phase and Ca associated with sodium nitrate.

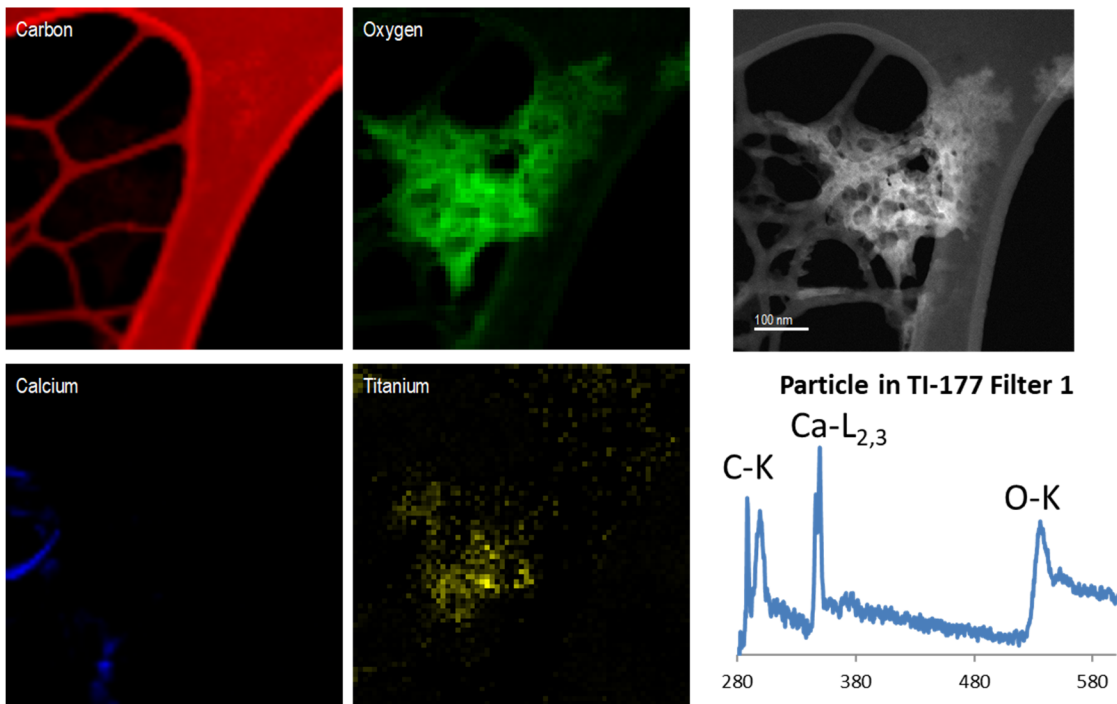


Figure E.6. STEM HAADF image and STEM-EDS maps of a calcite particle observed in Filtered Solution-1.

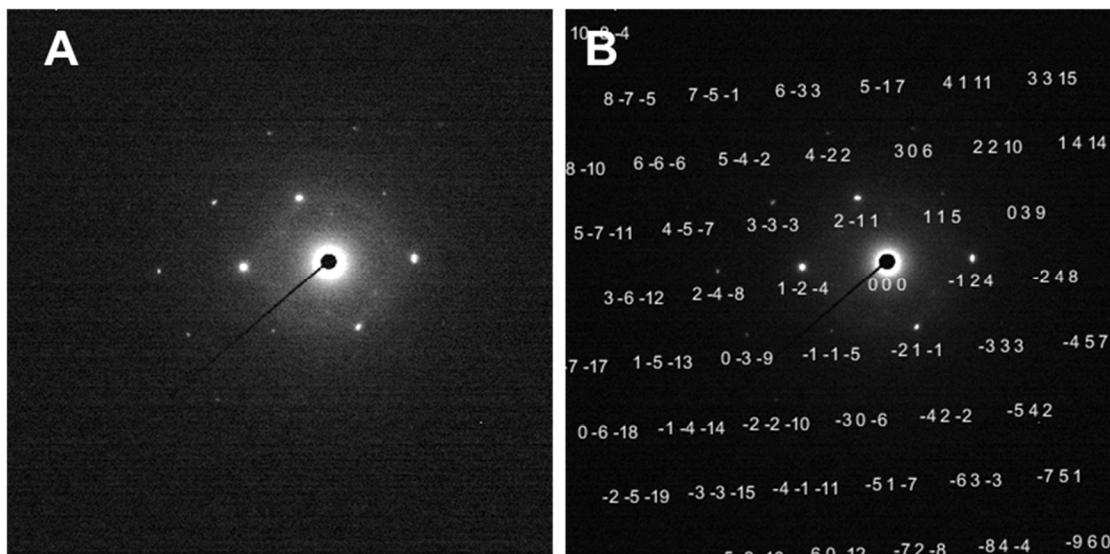


Figure E.7. (A) SAED from possible calcite phase and (B) identified as the $[-2-31]$ zone axis.

E.2.2.2 Uranium-Bearing Phase in Filtered Solution-1

Uranium phases were observed throughout the Filtered Solution-1 sample. Elemental maps in Figure E.8 show a bright region in the STEM-HAADF image that coincides with uranium. However, Fe, Ca, and Ni were also detected in this region. On closer inspection, the material appeared to be an oxide particle with a U-phase on one side and a Ca-bearing phase on the other side. Both TEM imaging with SAED (see Figure E.9) and higher magnification TEM-diffraction (see Figure E.10), and a high-magnification STEM-EDS image (see Figure E.11), were obtained from this particle. The STEM-EDS confirmed the phase as mainly U and O. The diffraction patterns were inspected and compared against clarkeite. Table E.2 lists d-spacings from the ring pattern and from the spot pattern. The phase had a reasonable match with clarkeite.

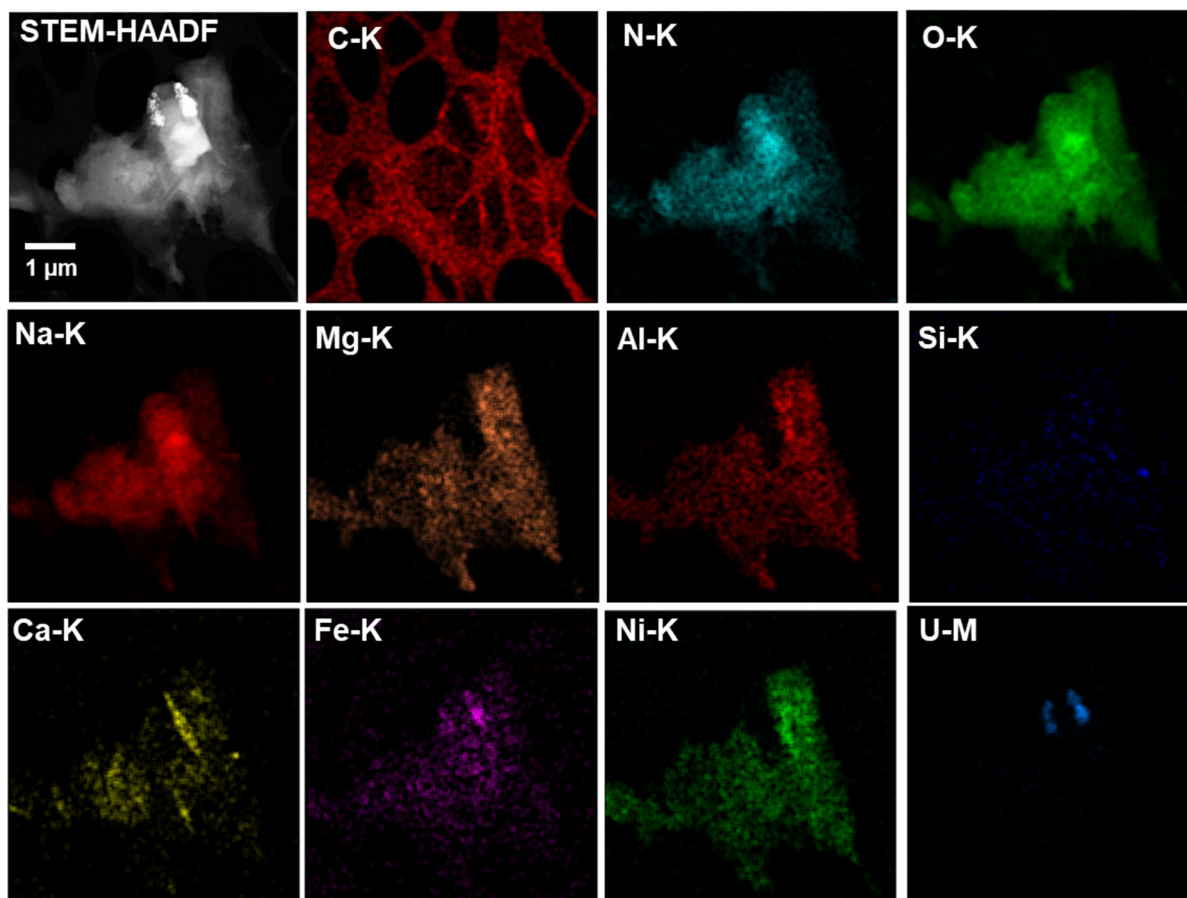


Figure E.8. STEM-EDS of particles from Filtered Solution-1 showing Ca fibers and a U-Fe particle.

The elemental map in Figure E.8 shows the holey carbon film that was used to capture the particles. The phase contained N, O, and Na, suggesting evaporite solids had formed; however, the presence of Fe, Ni, and U indicated the occurrence of an undissolved solid. The STEM-HAADF image also clearly indicated a high Z particle. The instrument was then run in TEM mode to capture a diffraction pattern and to obtain more detailed morphological information. These can be seen in Figure E.9A and C and Figure E.10A, where the U phase is darker because it is thicker (owing to the presence of U), but also because there was Bragg contrast (see Figure E.9C), indicating that the phase was crystalline. All the phases in these samples were beam sensitive and could be easily amorphized in the beam. Nevertheless, electron diffraction patterns were obtained (see Figure E.9B and Figure E.10B) and compared to clarkeite. The electron diffraction analysis was performed using CrysTBox (Klinger 2017). The high-resolution TEM image (see Figure E.9D) also indicates crystallinity in the uranium phase.

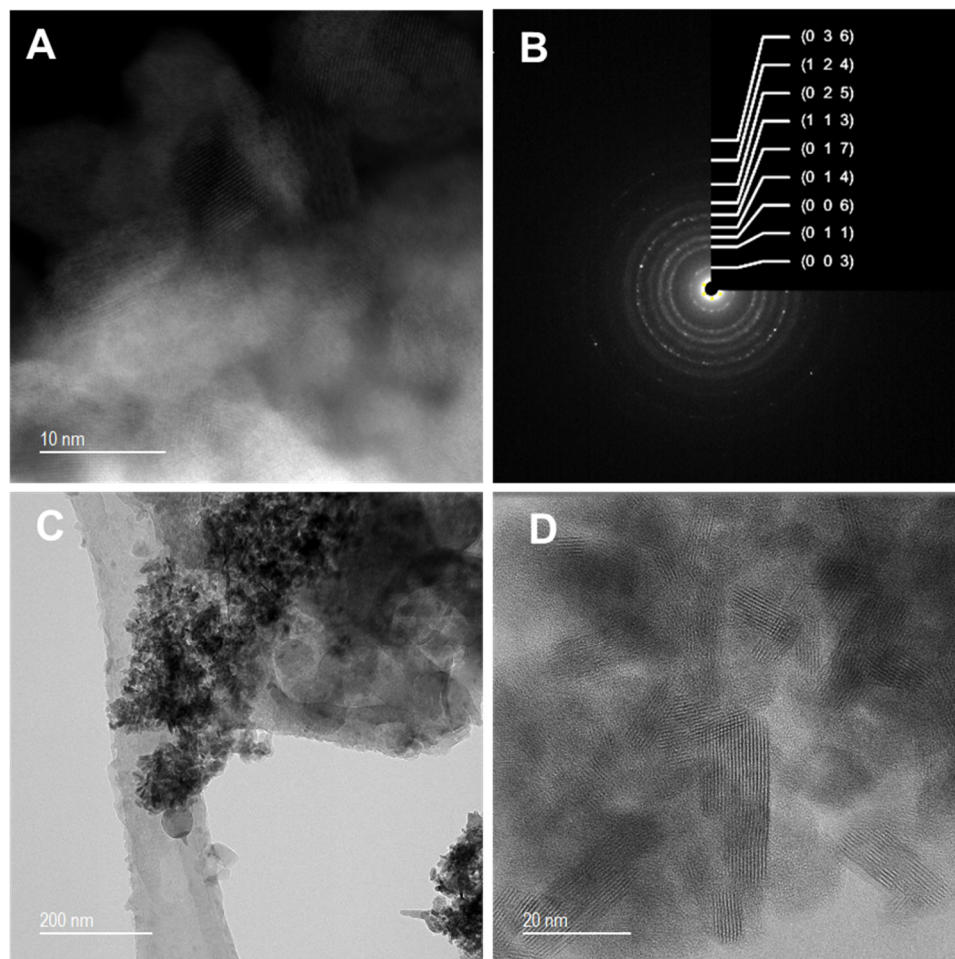


Figure E.9. TEM analysis and insert SAED of a particle observed in the Filtered Solution-1 sample.

The electron diffraction data is presented in Table E.2 and provides a good match to the clarkeite. Clarkeite was selected as this phase was previously identified in AW-105 with XRD ((Reynolds et al. 2014).

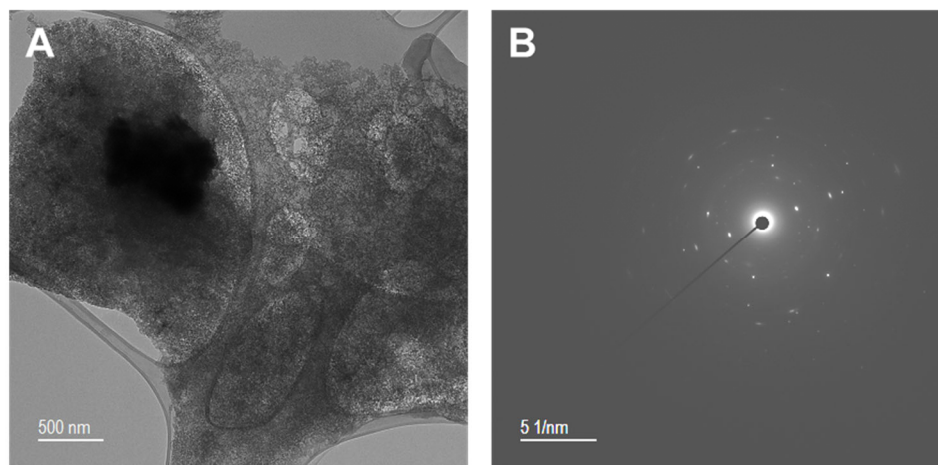


Figure E.10. TEM image and electron diffraction patterns obtained from a uranium-bearing particle in Filtered Solution-1.

Table E.2. Electron diffraction from Figure E.1 compared to clarkeite (Finch and Ewing 1997).

hkl Plane	d-spacing [nm]		hkl Plane	d-spacing [nm]	
	Theor. (Clarkeite)	Ring Pattern Observed		Theor. (Clarkeite)	Spot Pattern Observed
(0 0 3)	0.589	0.724	(0 0 6)	0.294	0.293
(0 1 1)	0.336	0.370	(0 1 7)	0.203	0.214
(0 0 6)	0.294	0.301	(1 1 3)	0.187	0.181
(0 1 4)	0.271	0.254	(0 2 5)	0.154	0.151
(0 1 7)	0.203	0.211	(1 2 1)	0.129	0.132
(1 1 3)	0.187	0.182	(1 2 4)	0.124	0.125
(0 2 5)	0.154	0.150	(1 2 4)	0.124	0.122
(1 2 4)	0.124	0.122	(0 4 7)	0.081	0.082
(0 3 6)	0.106	0.106			

The high-resolution STEM-EDS confirmed the composition of the phase with both O and Na present. It is only with TEM/STEM that such accurate data can be collected on these small phases.

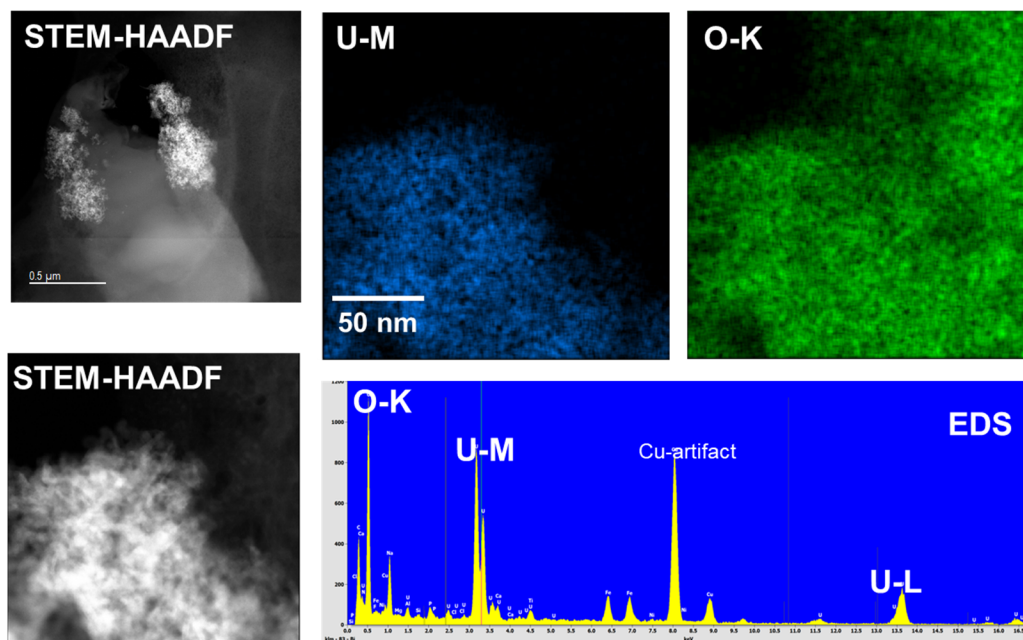


Figure E.11. STEM-EDS analysis of possible clarkeite uranium-bearing phase.

E.3 Conclusions on TEM/STEM analyses

This appendix provides data on sample segments from Hanford tank AW-105 that were examined with STEM/TEM analysis. Both Ca-bearing and U-bearing phases were observed, and these were identified as calcite and clarkeite, respectively. However, no Zr-bearing solids were observed with STEM/TEM in the filter solution specimens.

E.4 References

- Daniel, R. C., C. A. M. Burns, R. A. Peterson, V. L. Saldana, and N. L. Canfield. 2020. *Testing of an AP-105 Precipitation Simulant*. United States.
- DiCenso, A. T., L. C. Amato, J. D. Franklin, R. W. Lambie, R. H. Stephens, and B. C. Simpson. 1994. *Tank Characterization Report for Double-Shell Tank 241-AW-105*. Westinghouse Hanford Co., Richland, WA (United States); Los Alamos Technical Associates, Inc., Kennewick, WA (United States). United States.
- Downs, R. T., and M. Hall-Wallace. 2003. American Mineralogist Crystal Structure Database. <https://rruff.geo.arizona.edu/AMS/amcsd.php>.
- Finch, R. J., and R. C. Ewing. 1997. "Clarkeite; New Chemical and Structural Data." *American Mineralogist* 82 (5-6): 607-619. <https://doi.org/10.2138/am-1997-5-620>.
- Gehart, R. E. 2003. *Hanford: A Conversation About Nuclear Waste and Cleanup*. Battelle Press. <https://books.google.com/books?id=syFSAAAAMAAJ>.
- Herting, D. L., G. A. Cooke, J. S. Page, and J. L. Valerio. 2015. *Hanford Tank Waste Particle Atlas*. U.S. Department of Energy. LAB-RPT-15-00005; TRN: US1801801. Richland, WA. <https://doi.org/10.2172/1423895>.

- Klinger, M. 2017. "More Features, More Tools, More Crystbox." *Journal of Applied Crystallography* 50 (4): 1226-1234. <https://doi.org/10.1107/S1600576717006793>.
- Lumetta, G. J. 1994. *Pretreatment of Neutralized Cladding Removal Waste Sludge: Results of the Second Design Basis Experiment*. Pacific Northwest National Lab. (PNNL), Richland, WA (United States). United States.
- Mitchell, D. R. G. 2008. "Difftools: Electron Diffraction Software Tools for Digitalmicrograph™." *Microscopy Research and Technique* 71 (8): 588-593. <https://doi.org/10.1002/jemt.20591>.
- Peterson, R. A., E. C. Buck, J. Chun, R. C. Daniel, D. L. Herting, E. S. Ilton, G. J. Lumetta, and S. B. Clark. 2018. "Review of the Scientific Understanding of Radioactive Waste at the U.S. DOE Hanford Site." *Environmental Science & Technology* 52 (2): 381-396. <https://doi.org/10.1021/acs.est.7b04077>.
- Reynolds, J. G., H. J. Huber, G. A. Cooke, and J. A. Pestovich. 2014. "Solid-Phase Zirconium and Fluoride Species in Alkaline Zircaloy Cladding Waste at Hanford." *Journal of Hazardous Materials* 278: 203-210. <https://doi.org/10.1016/j.jhazmat.2014.05.097>.
- Ritenour G. 2006. Final Report For Tank 241-AW-105 Core 322 Samples For The Corrosion Mitigation And Criticality Programs. RPP-RPT-29745 Rev.0A. CH2M Hill, Richland, Washington.
- Sasaki, L. M. 1997. *Tank Characterization Report for Double-Shell Tank 241-AW-105*. Fluor Daniel Hanford, Inc., Richland, WA (United States). United States.
- Wells, B. E., D. E. Kurath, L. A. Mahoney, Y. Onishi, J. L. Huckaby, S. K. Cooley, C. A. Burns, E. C. Buck, J. M. Tingey, and R. C. Daniel. 2011. *Hanford Waste Physical and Rheological Properties: Data and Gaps*. Pacific Northwest National Laboratory (PNNL), Richland, WA (US).

Appendix F – Alpha Energy Analysis of Backpulsed Solids from AW-105

Pacific Northwest National Laboratory
Richland, WA
Radiochemical Sciences and Engineering Group

Filename: ASR 2198 Allred AmPu Report
 3/3/2025

Client: J. Allred Project: 84297
ASR: 2198 Charge code: NU8946

Prepared by: Lawrence R Greenwood
Digitally signed by Lawrence R Greenwood
 Date: 2025.03.14 14:14:38 -07'00'

Concur: Catalin Harabagiu
Digitally signed by Catalin Harabagiu
 Date: 2025.03.17 08:15:25 -07'00'

Procedure: Activity 7893, *Separation of Actinides and Sr using TRU Resin*
 Activity 6343, *Alpha and Beta Counting by GPC, LSC, and AEA*
 M & TE: AEA detectors
 Count date: 27-Feb-25

RPL ID:	Sample ID:	Pu-238, $\mu\text{Ci/sample}$		Pu-239/240, $\mu\text{Ci/sample}$	
25-0436	BDEF-AW5	1.80E-03	$\pm 2\%$	4.11E-03	$\pm 2\%$
25-0436 dup	Solids2	1.78E-03	$\pm 2\%$	4.14E-03	$\pm 2\%$
25-0431 PB		< 2.1E-08		6.51E-08	$\pm 28\%$
25-0431 BS				84%	
25-0436 MS				101%	

The Pu analyses were performed using a Pu-242 tracer. Results are reported as uCi per the entire sample that was received.

Pacific Northwest National Laboratory
 Richland, WA
 Radiochemical Sciences and Engineering Group

Filename: ASR 2198 Allred AmPu Report
 3/10/2025

Client: J. Allred Project: 84297
 ASR: 2198 Charge code: NU8946

Prepared by: Lawrence R Greenwood
Digitally signed by Lawrence R Greenwood
 Date: 2025.03.14 14:22:10 -07'00'

Concur: Catalin Harabagiu
Digitally signed by Catalin Harabagiu
 Date: 2025.03.17 08:13:45 -07'00'

Procedure: Activity 7893, *Separation of Actinides and Sr using TRU Resin*
 Activity 6343, *Alpha and Beta Counting by GPC, LSC, and AEA*
 M & TE: AEA detectors
 Count date: 27-Feb-25

RPL ID:	Sample ID:	Am-241, µCi/sample	
25-0436	BDEF-AW5	2.45E-02	± 2%
25-0436 dup	Solids2	2.45E-02	± 2%
25-0436 PB		1.35E-07	± 20%
25-0436 BS		90%	
25-0436 MS		76%	

*The Am analyses were performed using an Am-243 tracer. The tracer yield was an order of magnitude too high resulting in a very low matrix spike yield suggesting that the sample contained significant Am-243. Results were thus renormalized to 100% tracer yields for the sample. Results are reported as uCi per the entire sample that was received.

Pacific Northwest National Laboratory

902 Battelle Boulevard
P.O. Box 999
Richland, WA 99354
1-888-375-PNNL (7665)

www.pnnl.gov